CHALMERS

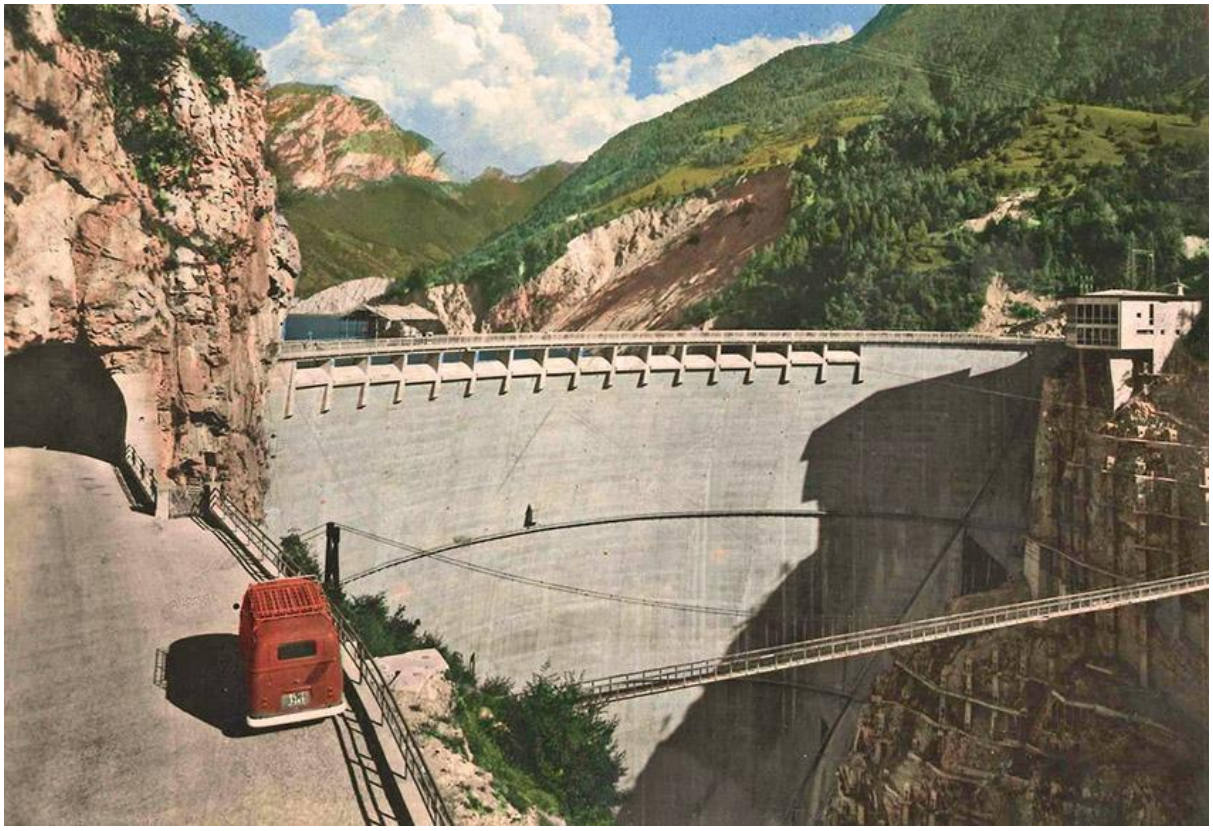

The Vajont slide

Facing the complexity of nature

Bachelor thesis in Geology and Geotechnics

ABDULRAHMAN AL SHAMAA
ALICE JOHNSSON
DANIEL WALLIN
MIA ENGMAN

Department of Architecture and Civil Engineering
CHALMERS UNIVERSITY OF TECHNOLOGY
Gothenburg, Sweden 2019

Bachelor thesis ACEX10-19-32

The Vajont slide

Facing the complexity of nature

ABDULRAHMAN AL SHAMAA
ALICE JOHNSSON
DANIEL WALLIN
MIA ENGMAN

Department of Architecture and Civil Engineering
CHALMERS UNIVERSITY OF TECHNOLOGY
Gothenburg, Sweden 2019

Sammandrag

Skredet i Vajont var en katastrof som inträffade i oktober 1963. Skredet genererade en våg som översteg dammens höjd och förstörde byn Longarone vilket dödade drygt 2000 personer. Denna rapporten undersökte anledningarna till skredet och effekten av höjningen och sänkningen av vattennivån på glidytan av Vajont. Utöver detta undersöktes mekanismerna kopplade till skredet i Vajont utifrån tre olika fall; 1) Mekanisk glidning; 2) Hydromekanisk glidning; och 3) Termomekanisk glidning. Dessutom genomfördes en litteraturstudie gällande dagens moderna standarder inom fältet för geoteknik, mildringsåtgärder och tidigare varningssignaler.

Resultatet från fallet med hydromekanisk glidning gav de mest framträdande resultaten då detta fall inkluderade fler parametrar såsom effekten av införd friktionsvinkel, snabb sänkning av vattennivån, hydrostatiskt vattentryck, kohesion och införandet av en upplyftande kraft. Utöver detta genomfördes en litteraturstudie som behandlade användningen av moderna standarder inom fältet för geoteknik och resultatet renderade ingen konkret slutsats. Detta berodde på komplexiteten av platsen ifråga och alla aktörer som var inblandade. Dock genomfördes åtgärder för att minska skadan av ett potentiellt skred, men dessa åtgärder var inte av tillräcklig omfattning för att förhindra katastrofen. Dessa åtgärder skapades som en respons på ett antal olika varningssignaler såsom en ökad hastighet av förskjutningen på skredet, ett antal stenras samt en spricka med en längd på 2 km. Rapporten presenterar ett antal förslag på åtgärder som hade kunnat mildra konsekvenserna av skredet. Exempelvis föreslogs en dräneringstunnel samt ett förslag rörande en generell sänkning av hastigheten för uppdämningen av dammen.

Abstract

The Vajont slide was a disaster that took place in October 1963. The landslide generated a wave which overtopped the dam, destroyed the village of Longarone and killed approximately 2,000 people. Attempts were made to mitigate the potential landslide, but these were not sufficient to prevent the disaster from taking place. These mitigations were created as a response to several warning signs such as increased landslide velocity, numerous rockfalls and a crack with a length of 2 km.

This thesis investigated the origins of failure and the filling-drawdown effects for the Vajont slide. In addition, the failure mechanisms of the Vajont slide were analyzed for three different cases; 1) Mechanical sliding; 2) Hydromechanical sliding and 3) Thermomechanical sliding. Furthermore a literature review regarding the current modern standards within the field of geotechnics, mitigation measures and the past warning signs was performed. The results from the hydromechanical case yielded the most extensive results since it included numerous parameters such as the effect of friction angle, rapid drawdown, hydrostatic water pressure, cohesion and uplift force. Furthermore, the literature study on the use of modern standards within the field of geotechnics and its application of the Vajont slide rendered inconclusive results. This is due to the complexity of the site itself and the actors involved.

Furthermore, a line of action is proposed that includes suggestions on preventive measures that could have been used to mitigate the consequences of the disaster. For example a drainage tunnel is proposed along with a suggestion to reduce the velocity of water impoundment in the dam.

Key words: Vajont slide, origins of failure, filling-drawdown effects, factor of safety, slope stability, mechanical sliding, hydromechanical sliding, thermomechanical sliding, thermal softening.

Table of contents

Preface

This Bachelor thesis was composed by four students at Chalmers University of Technology at the Department of Architecture and Civil Engineering. The project began in January 2019 and was completed in May 2019. During the entire time of the project Prof. Eleni Gerolymatou supervised the working process.

We would like to give special thanks to:

Carina Sjöberg Hawke, Fackspråk och kommunikation
Eleni Gerolymatou, Department of Architecture and Civil Engineering
Liza Nordfeldt, Bibliotekarie vid informationskompetens för lärande och forskning
Minna Karstunen, Department of Architecture and Civil Engineering

Gothenburg May 2019

Abdulrahman Al Shamaa
Alice Johnsson
Daniel Wallin
Mia Engman

Notations

Roman letters

a	Acceleration
c	Cohesion
D	Driving force
e	Thickness of shear band
h_w	Height of water level
i	Hydraulic gradient
L	Length of different sections
M	Frictional thermal parameter
N	Frictional rate-sensitivity parameter
P	Hydrostatic water pressure
q	Flow rate of water
Q	Water force
R	Resisting force
S	Degree of saturation
ΔS	Degree of displacement
t	Time
u	Pore-water pressure
U	Uplift force
V	Velocity
V_v	Total volume of voids
V_w	Total volume of water
W	Weight of rock mass
$\dot{w}$	Rate of work input per unit volume of band material
X	Frictional force

Greek letters

β	Slope inclination
ε	Inclination of rock mass
μ	Friction coefficient
ρ	Density of water
τ	Shear strength
σ	Total stress
σ'	Effective normal stress
φ	Angle of internal friction
$\dot{\gamma}$	Shear strain rate
θ	Temperature

1. Introduction

The Vajont slide is an example of a landslide of an enormous magnitude where the consequences of the disaster were both severe and prolonged and the lives of approximately 2000 people were lost (Petley, 2008). The construction of the Vajont dam and the filling of the reservoir contributed to this tragedy. Despite investigations and warning signs, the risks that were attached to the landslide were to some extent overlooked due to conflicting interests.

This case is still relevant today due to landslides being a contemporary issue. The problem of landslides, in general, is linked to the complexity of the number of stakeholders involved. For example economical, political, social and ethical interests interplay with different aims and visions for the project. This report will address the circumstances of the landslide including the warning signs, mitigations, modern standards and the mechanics involved. To better understand the circumstances of the landslide the report will include theory supporting the mechanisms.

1.1 Background

In 1939, at the commencement of the Second World War, Italy's GDP had dropped significantly (Rossi and Toniolo, 1996). As a result, there was a need to restore and stabilise the Italian economy during the post-war period (Bianchizza & Frigerio, 2013; Chernov & Sornette, 2016). The development of hydraulic works was part of the Italian government's nationalist programme (Bianchizza & Frigerio, 2013). The planning of the dam started in 1920, but residents in villages surrounding the valley did not hear of the project until 1958. SADE, Società Adriatica di Elettricità, a privately-owned electricity company, gained a permit for constructing the dam in 1943, mid-Word War II (Bianchizza & Frigerio, 2013).

This background will introduce the setting to gain an overview of the situation leading up to the landslide. Location and geological context and the line of events will provide knowledge of how the landslide was triggered.

1.1.1 Location and geological context

The Vajont dam is constructed in the Piave river which runs through the valley by the mountain Mount Toc located in the southeast Alps domain (Wolter, Stead, Ward, Clague & Ghirotti, 2019), figure 1. The Piave river runs through the town of Longarone and is surrounded by smaller villages such as Erto and Casso. The location of the dam in relation to the surrounding communities will later prove to be of crucial importance, with regards to the damage that was caused on each community.

Figure 1. The location of the Vajont dam. Author's own copyright.

Mount Toc, see figure 2, consists of limestones of the Fonzaso and Socchèr formations but also thin intercalations of clay (Wolter et al., 2019). The southern part of the village Erto syncline is an area with a high sensitivity of displacement (Massironi et al., 2013).

Figure 2. The area of the landslide, Mount Toc (Montagna, 2005). CC-BY.

1.1.2 Line of events

Excavations preparing for the construction of the Vajont Dam began in 1956, as can be seen in figure 3. The dam was fully constructed, and ready to be initiated with the three filling-drawdown processes on the 2nd February 1960 (Paronuzzi et al., 2013). In all the stages of the filling-drawdown procedures the rate of displacement and the amount of rainfall were observed. The observations took place in the southern part of Vajont because that was the most sensitive side of Mount Toc (Paronuzzi et al., 2013).

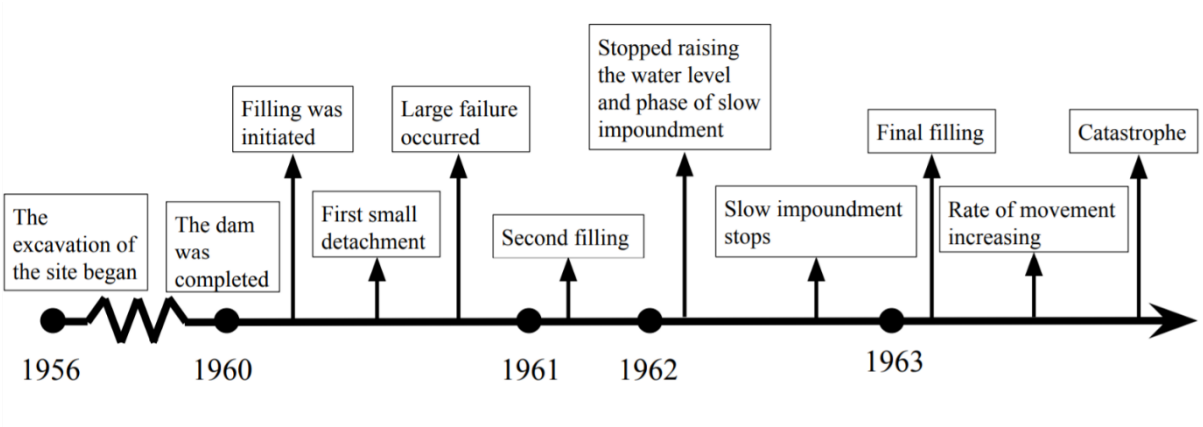

Figure 3. Timeline for the filling-drawdown process. Author's own copyright.

The first sign of concern was reported in March 1960 when the reservoir level had reached a level of 130 m, see figure 4. This led to numerous rockfalls nearby the so called Massalezza gorge. However, a much worse event occured in the very beginning of November 1960 when the water level had reached a level of 180 m (Petley, 2008). This formed an enormous crack of 2 km in length in the northern part of Mount Toc (Paronuzzi et al., 2013). The event occured whilst heavy precipitation was ongoing in the area. After this event the water level was dropped back to 135 m (Petley, 2008).

Between October 1961 and February 1962, the level of the reservoir was raised a second time after the initial filling. It was raised to an elevation of 185 meters, as can be seen in figure 4. The elevation of the reservoir increased to a level of 235 meters by November 1962. At that time, the velocity of the displacement of land mass had increased to 1.2 cm/day (Petley, 2008). The increase in the velocity of the displacement was regarded as a warning sign. As a response, the reservoir level was reduced to the former reservoir elevation of 185 meters to slow down the velocity of the displacement. This measure proved to be successful in the short-term and the velocity of the displacement was reduced to 0 cm/day. Engineers were now assured that they had been able to control the displacement by reducing the level of the reservoir (Petley, 2008). However, it was also noted that the behavioural response of the landslide was slightly paradoxical. The velocity of the displacement was much slower during the second filling, compared to the first filling of the reservoir (Müller-Salzburg, 1986).

The third and final filling, see figure 3 and figure 4, began in April 1963 (Paronuzzi et al., 2013). As mentioned earlier, the engineers thought that the displacement of the slope could be controlled. However, this theory failed in June 1963 when displacements increased steadily up to 0,3 cm/day. In July 1963 the movement increased to 0,5 cm/day and in August it reached 0,8 cm/day (Kilburn & Petley, 2003).

In September 1963 the velocity reached a very concerning magnitude of 3,5 cm/day and the reservoir level had increased to 245 m (Petley, 2008). Since this value of elevation and displacement exceeded previous records of average measurements, engineers decided to initiate a drawdown procedure of the Vajont dam. This was done in belief that lowering the reservoir would contribute to a decrease in the movement of the slope (Kilburn & Petley, 2003). However, the rate of the movements continued to increase and reached 20 cm/day (Petley, 2008). In comparison to the behaviour during the second filling, the behaviour of the landslide mass during the third filling was as expected (Müller-Salzburg, 1986). By the evening at 22:39 on the 9th October (GMT +1) the Vajont slide was initiated (Paronuzzi et al., 2013). Veveakis et al. (2007) claim that the landslide was caused by the filling of the reservoir coupled with external effects of rainfall and snowmelt.

A volume of 270 million $m^3$of rock displaced from the mountainside and reached a staggering velocity of 30 m/s (Kilburn & Petley, 2003). The sliding rock mass, with a length of 1700 m and 1000 m in width, plunged into the reservoir with force. The landslide remained intact and it generated a massive wave. The wave overtopped the dam and reached a maximum height of 260 meters and stretched to the other side of the valley. The village of Longarone was totally destroyed by this event while other villages were partly damaged (Müller, 1987).

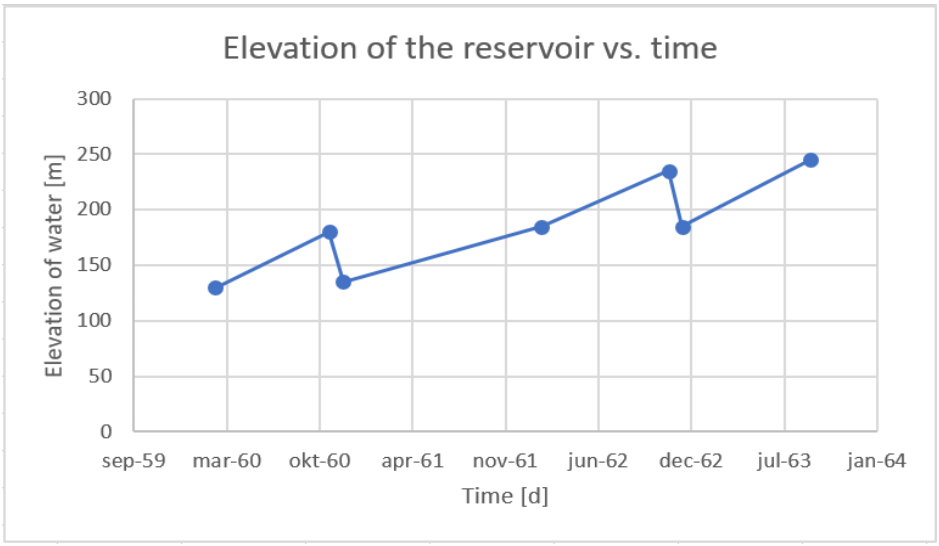

Figure 4. Variation of the water level of the Vajont Dam. Author's own copyright.

1.2 Purpose

The purpose of this report is to discuss and study the origins of failure and the filling-drawdown effects for the Vajont slide. Many scholars have suggested that the landslide could have been avoided if proper investigations and monitoring had been conducted. Therefore, the report will include a literature review discussing the warning signs that were overlooked and current modern standards that are in place to avoid disasters of this kind. A line of action will be discussed further in accordance with the preceding warning signs and contemporary modern standards. To create a better understanding for the failing mechanisms and the discrepancy of the research conducted in this area, the report will include three different analyses; 1) Mechanical sliding; 2) Hydromechanical sliding; and 3) Thermomechanical sliding.

1.3 Limitations

The disaster of the Vajont slide was a catastrophe triggered by many factors. One of these factors was the combined misconduct of the government and SADE, which did not clarify who was accountable if a disaster was to happen and, also, it gave little room for the local people to have a say in the matter. Many reports have discussed this matter, and even though this is an important subject, this report will not conduct an extensive ethical analysis of the Vajont slide. However, this matter will slightly be analysed in the discussion section of this thesis.

One of the limitations is related to the construction of the dam. The landslide did not have any direct correlation to the body of the dam, in fact the dam endured a load eight times greater than what it was dimensioned for. Therefore, no further investigation of the body of the dam will be carried through as that has no direct correlation to the landslide, which was the cause of the disaster.

The economical consequences of the disaster will not be covered in this report. It is an interesting point to consider but the main focus is the mechanical aspect of the catastrophe. Investments in geotechnical studies such as further extensive drilling prior to the disaster may have provided more information about the risk related to the landslide in advance. Additionally, the economic circumstances of the project are not applicable to this study since it has no correlation to the mechanics of the landslide itself.

It is possible to conduct an analysis of the Vajont slide using 3D geometry. However, this would require an advanced numerical analysis. Therefore, 3D geometry will not be considered.

The effect of precipitation and snowfall will not be taken into account in the three different cases. Only the effect of raising and lowering the reservoir will be the main factor contributing to the analyses presented in this report.

Characteristics related to the rock mass and the sliding surface such as permeability, tension cracks and stratification will not be within the scope the analyses presented. For example the entire weight of the rock mass will be based on a single value of unit weight, despite the natural variation of density in the limestone.

The conducted research provided in the literature of the Vajont slide will not extensively be compared to the output from the cases presented in this report. This is because most of the analyses in the research has different geometries compared to the calculations of this report. To conclude, the large number of simplifications in the cases would lead to inaccurate comparison with conducted research of the Vajont slide.

2. Theory

This chapter will explain theoretical aspects that are important to better understand the origins and mechanics behind the Vajont slide. Mechanical characteristics and processes related to landslides such as failure behaviour, simple mechanical sliding, filling-drawdown effects and thermomechanical aspects will be explained to create a general basis of knowledge for the reader. In addition, warning signs, mitigations and modern standards will be reviewed to better understand the case specific issues related to the Vajont slide. Despite these not being mechanical mechanisms they might also be rightfully considered as the origins of the failure.

2.1 Failure behaviour of a landslide

Landslides have caused many disasters and continue to do so. In order to prevent future landslides, it is important to understand the triggering mechanisms that cause landslides and the main types of rock slope behaviour (Huang, 2009; Paronuzzi et al., 2014). In the case of a landslide, failure occurs when the load exerted to a block exceeds the bearing capacity. At this point, the driving forces of the block have exceeded the resisting forces, which at a particular threshold value causes a failure and the block begins to slide (Highland & Bobrowsky, 2008). Failures of this kind are identified as either ductile or brittle in their behaviour. The character of landslide failure determines the predictability of the failure, which is important to prevent disasters.

Certain characteristics of rock materials determine whether the material behave as brittle or ductile. This behaviour affects the character of potential failure and deformation (Petley & Allison, 1997). It is better if the solid begins to flow, rather than break instantly. A brittle failure is much more abrupt and difficult to detect before failure compared to ductile failure. The failure range can be affected by both stress and temperature (Choo & Sun, 2018).

Landslide events can occur due to long-term destabilization. For example, long-term destabilization can be triggered due to saturation of weaker layers below the landslide (Highland & Bobrowsky, 2008; Prokešová, Medveďová, Táborík & Snopková, 2013). This long-term destabilization is exacerbated by brittle fracture damage and strength degradation, which can occur in different parts of the rock mass (Huang, 2009). Massive rock slope failure arises from brittle fractures. These brittle fractures are aggravated by extensional strain, which can create internal shear planes due to its interface with already existing discontinuities. Studies over the past two decades associate large-scale rock landslides with unexpected brittle failure (Huang, 2009). Deep-seated landslides are especially critical, since these landslides can cause a great deal of both direct and collateral damage as the landslide ruptures.

2.2 Factor of safety

The factor of safety is the relationship between the critical and the tolerated loading (”Säkerhetsfaktor”, 2019). For a sliding mass the factor of safety can be defined as the ratio of the resisting and the driving force (Pariseau, 2011), see figure 5. Figure 5 can be expressed as components in a static model (Sällfors, 2013), see figure 6.

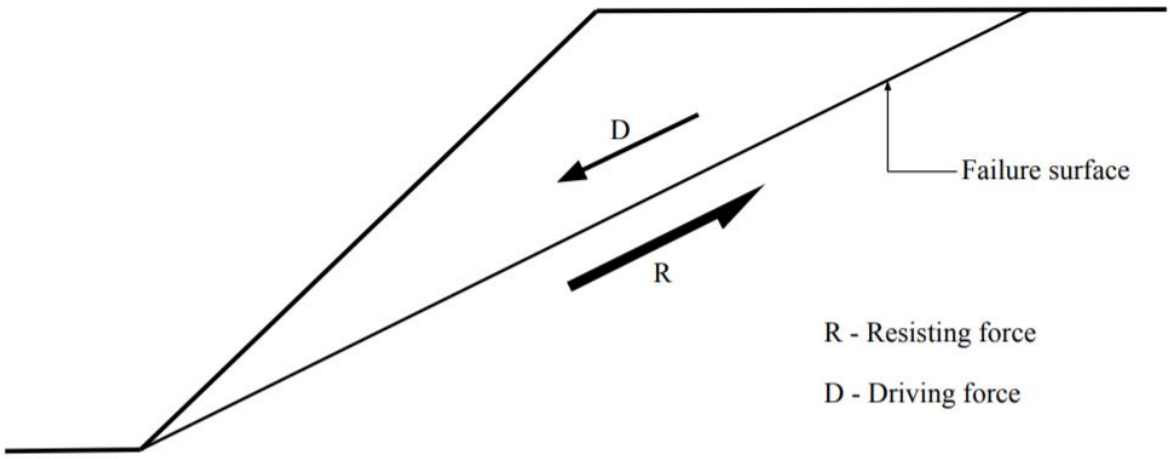

Figure 5. Illustration of the driving and resisting forces of a landslide. Author's own copyright.

These models generate an equation for the factor of safety, *FS*, see equation 1. Additionally, the friction coefficient, μ, generates the friction force. Finally, the gravity is multiplied with the angle of the plane, β, to obtain the components of the force in the right direction. As can be seen in the equation below, the area of the block and the mass, both in the numerator and denominator, cancel each other out. This yield $\frac{cos(\beta)}{sin(\beta)} = cot(\beta) = \frac{1}{tan(\beta)}$. Note that no cohesion is considered in this equation.

$$FS = \frac{\mu \cdot mg \cdot cos(\beta)}{A} \cdot \frac{A}{mg \cdot sin(\beta)} = \frac{\mu}{tan(\beta)} = \frac{R}{D} \qquad (1)$$

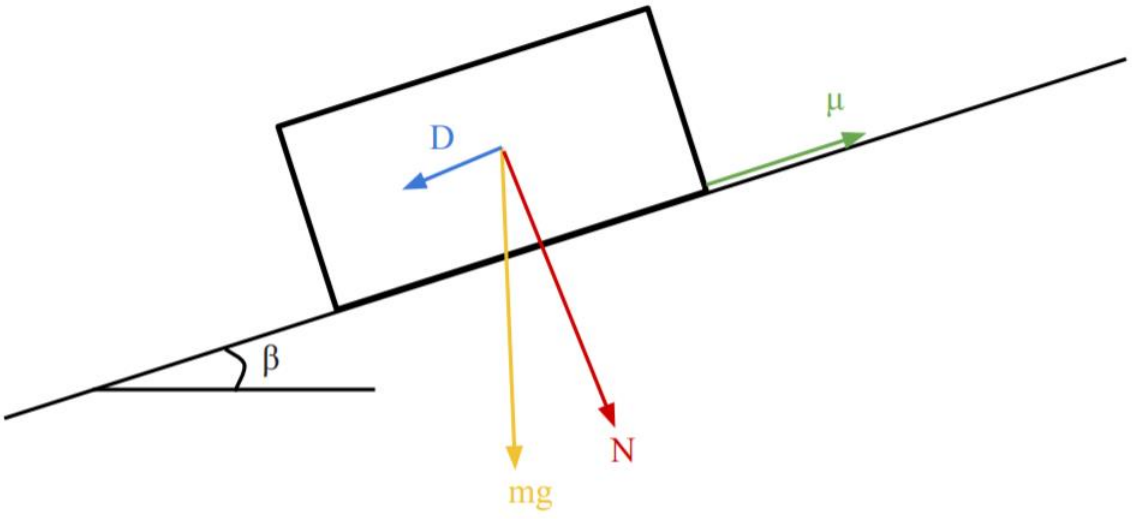

Figure 6. Illustration of the equilibrium forces for a sliding mass. Author's own copyright.

The use of Newton's second law yields:

$$F = m \cdot a \tag{2}$$

For the case of a block sliding along a failure surface the equilibrium can be rewritten as following:

$$F = D - R \tag{3}$$

Inserting equation (1) into equation (3) generates equation (4):

$$a = g(sin(\beta) - \mu cos(\beta)) \tag{4}$$

In order to obtain values of the displacements after the factor of safety is exceeded the following equation will be used:

$$\Delta S = a \cdot t^2 \tag{5}$$

Which describes the displacement, S $[m]$ in terms of velocity, a $[m/s^2]$ and time, t $[s]$.

Another equation will be used in determining the relationship between acceleration, time and velocity:

$$a = \frac{\Delta V}{\Delta t} = \frac{V_2 - V_1}{t_1 - t_2} \tag{6}$$

2.3 Mohr-Coulomb

Mohr-Coulomb is a mathematical model that has been, and is still used, for soil and rock. The model defines the shear strength at different effective stresses, as seen in figure 7.

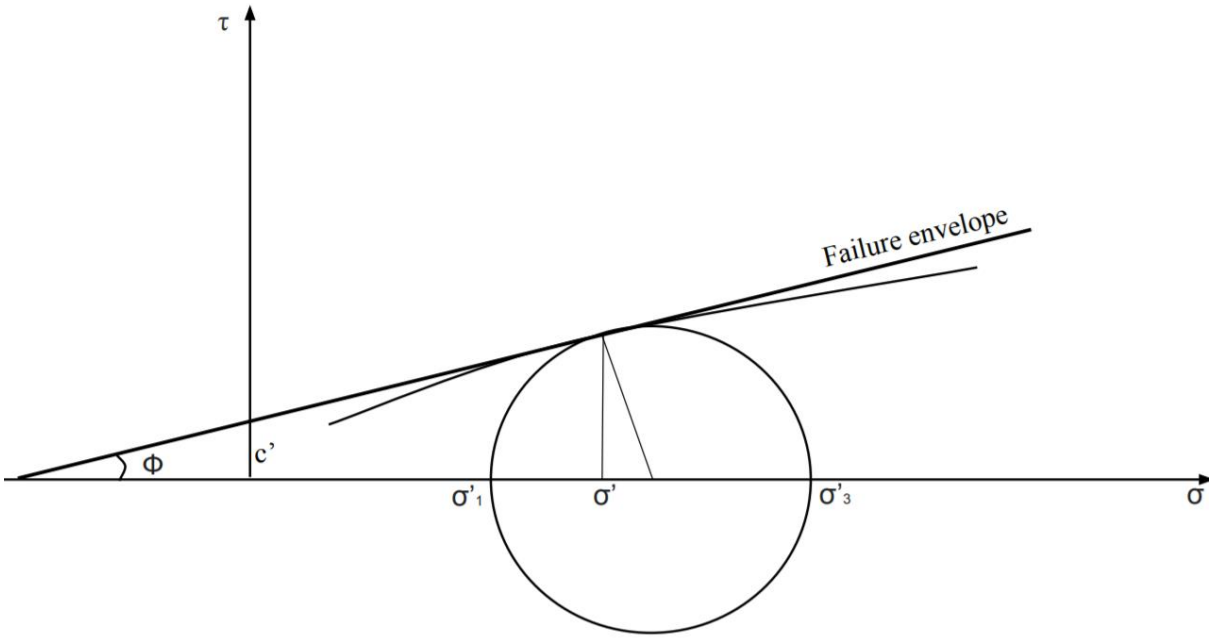

Figure 7. The Mohr-coulomb failure criterion. Author's own copyright.

The non-linear part of the failure envelope can be difficult to approach and is therefore estimated by a straight line. The failure criterion for Mohr-Coulomb is defined as a linear envelope (Craig & Knappett, 2012), as can be seen in figure 7. The connection between the shear strength and normal stress is defined as:

$$\tau = \sigma' \cdot tan(\phi) + c' \qquad (7)$$

where τ is the shear strength, σ' is the effective normal stress, c' is the effective inherent shear strength, also known as the cohesion, ϕ is the angle of internal friction and $tan(\phi)$ is the slope of the failure envelope, in the $\tau - \sigma$-plane. The soil or rock will reach failure in one single point (Craig & Knappett, 2012), where the circle touches the failure envelope.

2.4 Kinematics

Kinematics describes the movement of bodies without regard to the causes of the movement ("Kinematik", 2019). The fundamentals of kinematics are position and time, how the position of a point on a body depends on the time ("Kinematik", 2019; Waldron, Kinzel & Agrawal, 2016).

If one understands how landslides move and which mechanisms are the cause of these movements, one can predict the danger that landslides can pose. In the case of landslides, the origins of the movement have to be taken into account as well as the pure case of kinematics. Therefore the next subchapter will explain the different causes for the movement of a landslide.

2.4.1 Simple mechanical sliding

In order to understand the character of a landslide, it is important to understand its mechanisms (Stead & Eberhardt, 2013). Understanding mechanisms in large landslides includes the study of different possible failure mechanisms and their corresponding processes (Stead & Eberhardt, 2013).

Failure in a slope can be initiated due to tectonic damage or temporary conditions such as water pressures (Stead & Eberhardt, 2013). The failure surface geometry considered is therefore important to mention when discussing rock slopes since it determines how the slope will react to the conditions mentioned (Stead & Eberhardt, 2013). Huang (2013) writes that there are three types of failure surfaces, which are presented in figure 8.

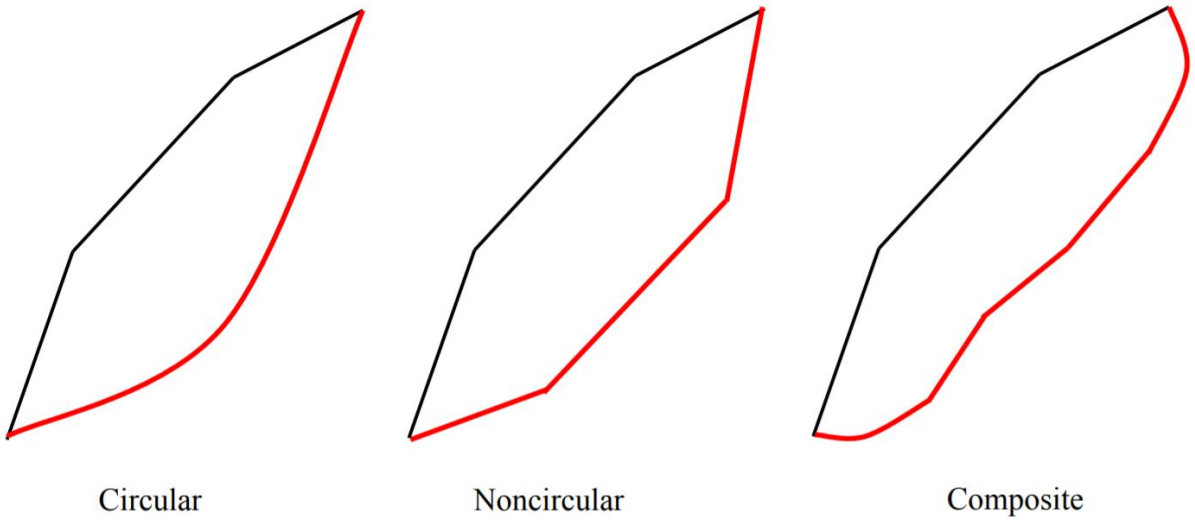

Figure 8. Failure surface geometry. Authors own copyright.

The first type of failure surface, see figure 8, is the circular failure which is also called the cylindrical failure surface. This type of failure surface occurs if the materials in the slope are homogeneous with no weak layers (Huang, 2013). The second type is the non-circular failure surface. It consists of a series of planes which explains why it is also known as a plane failure surface. The failure surface will occur at a point when the critical failure surface is located along the bottom of the weaker layers. This occurs if weak layers exist at the start or end of the slope surface (Huang, 2013). The last type of failure considered is the composite failure which is circular and defined as a partially plane failure surface. It is plane because the failure surface will follow the point of weakest strata when the circle cuts a layer of weak material (Huang, 2013).

Furthermore, the rock mass quality and rock slope kinematics have a major impact on rock slope failure. This highlights the importance of rock mass quality and its distribution. If the rock mass quality is unevenly distributed, such as in the case of the Vajont slide, the different rock masses will react differently to stress and disturbances creating failure (Stead & Eberhardt).

2.5 Impact of water

In general, the effect of water flowing through a slope is a rather complicated matter (Li & Liu, 2015). Water can affect parameters such as pore-pressure, groundwater table, reduction of soil suction and the shear strength of a soil. Since water is generally considered to be a huge contributor to landslides, it is of high importance to establish the fundamentals of water effects on slope stability.

One parameter that influences the properties of a material is the degree of saturation (Sällfors, 2013). It is defined as the percentage of water that is present in the pore spaces in a given material. A soil is fully saturated if all the pores are filled with water. If some of the pores contain air and others contain water, it is known to be partially saturated. The equation that describes this property of a soil is the following:

$$S = \frac{V_w}{V_v} \tag{8}$$

where V_w is the volume of water and V_v is the total volume of voids. Values of S range between 0 % to 100 % (Sällfors, 2013).

Another aspect to take into consideration in slope stability is water flow (Craig & Knappett, 2012). In a one dimensional fully saturated soil it is defined by Darcy's law:

$$V_f = k \cdot i \; or \; q = V \cdot A = A \cdot K \cdot i \tag{9}$$

Where q $[m^3/s]$ is the flow rate of the water, k is the permeability $[m/s]$, A is the cross-section area $[m^2]$, $i = \frac{\Delta h}{\Delta L}$ describes the hydraulic gradient $[-]$ and V_f is the flow velocity $[m/s]$ (Craig & Knappett, 2012). The driving force for water flow is the difference in hydraulic

pressures. Water moves in the direction of higher to lower total water head. (Cheremisinoff, 1998).

For the calculations presented in this report the fundamental equation for hydrostatic water pressure increase with depth will be used:

$$P = \rho \cdot g \cdot h_w \tag{10}$$

where P is the evaluated hydrostatic water pressure $[Pa]$, ρ is the density of water $[kg/m^3]$, g is the acceleration of gravity $[m/s^2]$ and h_w is the considered water depth $[m]$.

2.6 Filling-drawdown effects

Fluctuations in the water level of a reservoir or a slope are due to natural phenomena such as heavy rain or in other cases it might be an effect of human activities. Since water flow, pore-pressure changes and water loading leads to variations in effective strength and other soil parameters, its influence must be investigated. Therefore, in this chapter, the basic effects of filling-drawdown cycles on aspects such as pore-pressure will be discussed, to better understand the outcome of the Vajont slide.

2.6.1 Rapid drawdown

In general, drawdown of a water table is likely to impact the factor of safety of a slope (Johansson, 2014). Especially the case of rapid drawdown is a major contributor to differences in hydraulic gradients. When the water table is lowered it also tends to have a different type of effect, namely a reduction in the supporting water load (Johansson, 2014).

Several researchers have conducted experiments to quantify the effects of rapid drawdown of a water table and how it affects the slope stability. Yang et al. (2010) conducted an experiment including two one-meter high soil columns with clayey sand over medium sand and silty sand over fine sand. The results of this experiment were that in both soil columns there was a similar result in terms of changes in pore pressure. The pore-pressure changed very drastically immediately after the water table was lowered in both cases (Yang, Xiao, & Yang., 2010). It was also concluded that pore pressures remained at a high level immediately after the rapid drawdown was initiated (Johansson, 2014).

Hence it can be concluded that a rapid lowering of the water level impacts the factor of safety, generates differences in hydraulic gradients, reduces the supporting water load and it develops excess pore-pressures in a slope.

2.6.2 Increasing the water level

Another important aspect to consider is the effect of increasing the water level in reservoirs. Cai and Cojean (2011) presented a study of the Three Gorges Dam where it was concluded that rising water levels contributed to a decrease in the factor of safety. The water level has an additional load effect and leads to other issues such as induced seepage and a decrease in

negative pore-pressures. These factors have been linked to slope failure, settlement issues and a decrease of the shear strength in slopes (Johansson, 2014).

One experiment has been performed to quantify the effect of water level rise on a slope with dimensions 15 x 6 x 5 m (Chen, Fredlund, Jia & Zhan, 2009). This is many orders of magnitude lower compared to the Vajont slide but it is applicable to understand the fundamental effects of water level rise. The sample itself consisted of sandy-silty material (Jia et al., 2009).

During the raising of the water level the material under the sloping surface started to fail (Jia et al., 2009). The water-flow into the soil bank initiated a wetting-induced collapse. This in turn led to losses in shear strength which was linked to decreasing matric suctions. The water-level rise also influenced the friction angle leading to a reduction from 45 degrees to 33 degrees.

Hence it may be concluded that increasing the water level in a reservoir reduces the friction angle, decreases the factor of safety, contributes to an additional load effect and induces seepage in slopes.

2.7 Thermomechanical aspects

The addition of the concept “thermo” to “mechanics” describes how thermal energy affect certain mechanical properties. The amount of temperature determines how materials react to applied forces, which in turn affects their resultant motion (Regenauer-Lieb, Hobbs, Ord & Yuen, 2007).

2.7.1 Basic thermomechanics

Mechanical processes depend on force systems in equilibrium. These forces can be affected by the production and reduction of heat. Different materials have different heat capacities, meaning that the amount of energy required to increase the temperature of the material with 1˚C varies. Hence, material properties influence the heat production capacity and are key to both predict and analyse the resultant motion that is affected by the change of temperature of a material (Noll and Seguin, 2010). However, this requires input data to yield results.

To analyse a sliding mass the landslide can be assumed to act as a solid body of mass, with a considered velocity V_{max} (Alonso, 2010). 2e represents the thickness of the shear band. V_{max} is concentrated on the shear band. This results in an average shearing strain rate according to the equation below:

$$\dot{\gamma} = \frac{v_{max}}{2e} \tag{11}$$

The rate of work input per unit volume of the band material is calculated by the equation below. All of the work input will be converted into heat in the equation considered. As a result, the temperature of the landslide will increase, which in turn increases the excess pore water pressure. The excess pore water pressure increases as the water evaporates, which ultimately means that the volume of the water increases and, therefore, the pressure increases. Hence, the heat generated is dependent on shear strength, velocity and the thickness of the shear band.

$$\dot{w} = \tau_f \dot{\gamma} = \frac{\tau_f V_{max}}{2e} \quad (12)$$

2.7.2 Thermal softening

The sliding of a rock mass produces local heat on the slip surface (Habib, 1975). The heat is produced from the work generated by gravity forces. This heat induces the vaporisation of the pore water if the depth of the failure surface is sufficiently deep (Habib, 1975). The vapour contained inside the rock will further lubricate the motion. Meanwhile, the friction coefficient remains constant, while the shearing resistance is reduced due to the reduction in effective normal stress. The sliding movement of a large mass can produce much heat, which is generated by the friction between the mass and the planar surface. Alonso et al. (2010) claim that water boils at a temperature of 200 ˚C when the water pressure is estimated to 1.2 MPa. However, Voight and Faust (1982) argue that thermal softening does not require vaporisation of water, but merely a change in pore water pressure. Hence, a complete scientific consensus regarding the catalytic factors enabling thermal softening does not exist.

The shear strain rate is defined by the equation below which can be found in Veveakis et al. (2007). The equation explains the extent of the deformation depending on change in θ , temperature, whereas θ_1= 22 ˚C remains constant. Hence, it defines how the process of thermal softening either reduces or increases the strain rate.

$$\dot{\gamma} = \dot{\gamma}_0 \cdot e^{-M(\theta-\theta_1)} \quad (13)$$

$(\frac{\dot{\gamma}}{\dot{\gamma}_{ref}})^N$ is the strain ratio, the change in deformation, with respect to time and N is a frictional rate-sensitivity parameter that has to be taken into account (Veveakis et al., 2007). The equation below describes the shear stress,τ, in relation to in-situ effective stress,σ_0', and the friction coefficient. $\mu_{ref}$is the reference friction coefficient and M is a frictional thermal parameter.

$$\tau = \sigma_0' \cdot \mu_{ref}(\frac{\dot{\gamma}}{\dot{\gamma}_{ref}})^N \cdot e^{-M(\theta-\theta_1)} \quad (14)$$

2.8 Modern standards

In this report modern standards are regarded as recently developed technologies in the field of geotechnical construction. These technologies have been created to monitor landslides and to better understand earth phenomena, as earthquakes, that could trigger landslides to minimise the risk and improve disaster mitigation (Scaioni, 2015). This chapter will present some of the contemporary techniques that were not invented at the time of the Vajont slide.

2.8.1 Ground-based monitoring techniques

One of the ground-based monitoring techniques is close-range photogrammetry, CRP. This technique measures the deformation of a landslide by photographing the area and recreating a 3D-model of the landslide. This method is used for surface point tracking and comparison of surfaces obtained from dense image matching (Scaioni, 2015). CRP can reduce the time-consuming process of collecting data for landslides, however the results of the technique depend on the camera that is used (Abbaszadeh & Rastiveis, 2017). Another technique is a fixed Terrestrial photogrammetric system (Scaioni, 2015). The system is a tool that provides information on discontinuities and slope geometry (Fripo, Salvini, Francioni & Ranjith, 2011). This technique intents to directly or indirectly control the movement of the landslide by installing sensors whose movement can be detected in specific points (Scaioni, 2015).

Scaioni (2015) also discusses remote-sensoring techniques for rockfall risk assessment. This technique enables the characterisation of the main joints. Data on mechanical properties can also be measured and by using geometrical analyses unstable blocks and cliffs can be identified.

Terrestrial laser scanning (TLS) is considered an effective method for monitoring landslides (Scaioni, 2015). It is regarded as straightforward and it can collect a great deal of data in short time. It is a technique useful for measuring deformation in landslides with steep slopes and difficult terrains.

2.8.2 Geophysical and geotechnical Methods

The study of passive seismic earth movement allows for examination of internal cracks within a rock mass (Scaioni, 2015). There are different purposes for using passive seismic monitoring, it can be used for studying the source itself or to get an image of the surrounding (Al-Anboori & Kendall, 2010). For example, these purposes can be earthquake monitoring, reservoir hydrofracturing monitoring, landslide and rockfall monitoring. By placing sensors inside of the rock mass and on the surface, and then analysing the movement of the rock mass it produces information on where the risks for rockfall and landslides are located (Scaioni, 2015).

According to Scaioni (2015) flow-slide propagation is a reliable technique to minimize landslide problems in mountain areas. In the case of a steep slope, less water pressure can trigger the landslide, but in the case of a gentle slope the added saturated soil might trigger the landslide, this can make the landslide move in a flow-like motion (Beddoe & Take, 2015). This technique to minimize this problem is to monitor the shear induced pore water pressure or to evaluate the mobility of the flowside (Beddoe & Take, 2015).

2.9 Warning signs

Mount Toc was often referred to as the "Walking Mountain" by the local people of the area (Chernov and Sornette, 2016). It had gained its reputation due to its proneness to landslides in the past and present. Several events that led up to the catastrophe will be reviewed in this chapter and the coined popular name for Mount Toc will prove to have significance. Many of these red flags will be covered in text and in an illustrated timeline in figure 9.

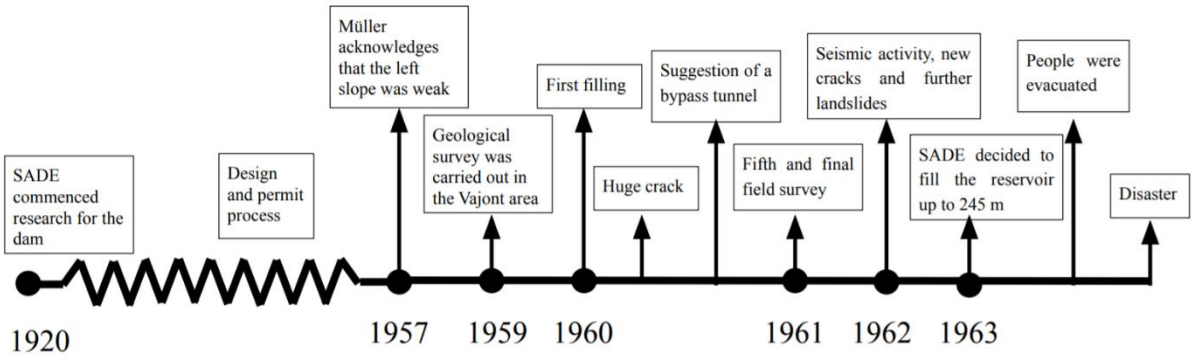

Figure 9. Timeline including some of the most critical events leading up to the landslide. Author's own copyright.

2.9.1 Indications of concern pre-finalisation of the Vajont Dam

SADE commenced research for the Vajont Dam between 1920 and 1928. The geologist, Giorgio Dal Piaz, was employed by SADE and was involved in the project the entire time (Genevois & Tecca, 2013; Barrotta & Montuschi, 2018). Carlos Semenza was the chief engineer who designed the Vajont Dam (Barrotta & Montuschi, 2018). In literature, Dal Piaz and C. Semenza are recurring names and often held accountable, thus, their names are worth mentioning. The design and permit process for the dam was carried out between 1925 to January 1957 (Genevois & Tecca, 2013). On the 6th August 1957 Müller acknowledges that the rock mass on the left slope of the valley was weak in its properties, which poses a risk to the establishment of the construction (Genevois & Tecca, 2013).

Many geologists and engineers were involved in the design, construction and risk analysis of the dam. The irregular shape of the syncline was expected to act as a break for any potential movements (Genevois & Ghirotti, 2005). Therefore, they were certain that a slope collapse was very unlikely (Genevois & Ghirotti, 2005). During this time, research regarding slope stability of reservoir valleys was seldom included in the planning phase and geology was not considered a concrete division of science (Semenza & Ghirotti, 2000; Barrotta & Montuschi, 2018). Therefore, the research conducted was not enough (Semenza & Ghirotti, 2000).

In 1959, a geological survey was carried out in the Vajont area (Semenza & Ghirotti, 2000). This was urged due to a landslide in the Maë valley, which occurred on 22nd March 1959 (Mantovani & Vita-Finzi, 2003; Semenza & Ghirotti, 2000). The Maë is a branch of the Piave River north of Longarone, not far away from the Vajont area. The geological survey led to the discovery of several ancient landslides, whereas one of these was recognized as potentially unstable. The existence of these much older landslides confirmed that the rock mass had moved

in the past (Semenza & Ghirotti, 2000). By 1959, the designers and constructors knew that it had existed large scale movements in the past. It was recognised that there was risk attached to the scene of the projects, however, the project carried on regardless. To better control the situation, it was decided that the movement in the landslide would be monitored during all the filling stages (Mantovani & Vita-Finzi, 2003).

While the construction began in January 1957, the High Council of Public Works appointed a committee "Commissione di Collando" to inspect the construction as late as in July 1958 (Genevois and Tecca, 2013). The "Commissione di Collando" carried out field surveys and the second one took place after the finalization of the dam.

2.9.2 Indications of concern post-finalisation of the Vajont Dam

After the construction was finalized in September 1959 another four field surveys were conducted. The first filling of the Vajont reservoir started in February 1960. During the months that followed, several rockfalls appeared on the slopes of the northern toe at Mount Toc (Paronuzzi et al., 2016). These sort of rock failures usually indicate brittle behaviour and this behaviour is often paired with microseismicity (Paronuzzi et al., 2016). In June 1960, E. Semenza and Giudici distinguished the presence of an ancient deep landslide at the left slope, based on past field surveys. They argued that the ancient landslide could be triggered by an increase in pore pressure (Barrotta & Montuschi, 2018). However, Dal Piaz, disregarded the ideas of E. Semenza and Giudici. Based on his research he determined that there were only minor and slow events of displacement.

An alarming event occurred in October 1960. On the slope of Mount Toc a 2 kilometer crack created a gap over an extensive area (Petley, 2008). To better understand why the crack had taken place a deep geological survey was carried out by several specialists. This research led to the belief that the different parts of the landslide would slide at different points in time, due to their varying properties and that these parts could be somewhat controlled. In November 1960, Semenza and Müller, among others, suggested a bypass tunnel to better control the water level in the eastern reservoir (Barrotta & Montuschi, 2018). However, before the bypass tunnel was completed, local newspapers reported on the matter in February 1961, and at the same time Müller estimated a $2 \cdot 10^8$ m^3 landslide, which would be impossible to stabilize. Research during 1961 from other specialists seems to conclude that the issue at hand was a shallow landslide, not a deep one as suggested earlier by Semenza and Giudici. As for the fifth and final field survey carried through on the 17th October 1961, by the "Commissione di collaudo", it established that the filling of the reservoir could go on, but circumstantial displacements cannot be ruled out (Barrotta & Montuschi, 2018).

In 1962, there was more seismic activity, new cracks appeared and further landslides took place (Semenza & Ghirotti, 2000). At the time many of these events are attributed to natural phenomena. Despite the justification of these events, SADE raised the issue of a possible evacuation of the Mount Toc area. Despite past events, on 22nd July 1963 SADE called for the filling of the reservoir up to 245 m. What followed was another seismic shake, several large fissures, displacements and drawdown of the reservoir. People living on the sliding slope were

evacuated on 7th October 1963 and on 9th October 1963 the disaster became a fact (Barrotta & Montuschi, 2018; Marco, 2012).

2.10 Mitigations

This chapter has so far covered the warning signs and the list of those are rather extensive. However, the list of mitigating measures is shorter. This is because while certain red flags were taken into account, others were not. The following chapter will review the mitigating processes that followed parallel to the filling and usage of the dam, as well as explain the two main mitigating measures: the drawdown and the bypass tunnel.

2.10.1 Drawdown

The water elevation in the reservoir was altered to control the surrounding landslides. It was altered by filling-drawdown cycles, which commenced on 2nd February 1960 (Paronuzzi et al., 2013). The pace of the filling and drawdown velocity varied over time. At this point during the operation of the dam there was a lack of deeper understanding of the hydrogeological structure of Mount Toc (Paronuzzi et al., 2013). Therefore, the filling and drawdown velocities were arbitrarily decided upon. Groundwater data was introduced to the project in the summer 1961. Despite the newly acquired data it was not used as input to the operation.

In November 1960 a slow-paced drawdown of the reservoir was initiated. The reservoir level was lowered to 170 m and this level was maintained until October 1961. This action was necessary for the later construction of the bypass gallery, which is covered in the following chapter. During the entire operation of the Vajont Dam the reservoir level was consistently raised and lowered in an attempt to control the sliding events that happened more frequently. In 1962, the level of the reservoir was raised in order to better predict the landslide displacements (Marzocchi et al., 2012). It was increased slowly and reached 235 m by late November 1962 (Havaej et al., 2015). The result of this conduct was a large increase in sliding movement in December 1962 (Marzocchi et al., 2012). In September 1963, the level had increased to 245 m, while the velocity had increased to 3,5 cm/day (Petley, 2008).

2.10.2 Bypass tunnel

As a reaction to the extensive landslide, which took place on 4th November 1960, a bypass tunnel was suggested on the 15th-16th November 1960. A new geoseismic instrument was also installed to better monitor the seismic activity that had been increasing (Havaej et al., 2015). The bypass tunnel was constructed in the northern part of the valley. The construction commenced in January 1961 and was accomplished in 1961. The purpose of this was to better control the water elevation as suggested by Semenza and Müller (Barrotta & Montuschi, 2018).

3. Method

The method will consist of three mechanical applications to the Vajont slide. It will be divided into three different cases and each case will employ a particular method; 1) Mechanical sliding; 2) Hydromechanical sliding; and 3) Thermomechanical sliding.

3.1 Case 1 - Mechanical sliding

This case will address the simple mechanics of the Vajont slide. Aspects such as velocity, acceleration and displacement of the landslide will be analysed in this chapter since they are all intertwined. To understand the magnitude of the disaster it is essential to study the mechanical properties.

3.1.1 Input parameters

The following input parameters were inserted to calculations of the Vajont slide based on values acquired from different reports. The values of mass, specific weight and the inclination of the slope were gathered from Alonso et al. (2010). Values concerning maximum displacement and maximum velocity were collected from Müller (1987). The value for the length of the landslide was collected from Paronuzzi and Bolla (2012). Finally, the value for the friction coefficient was obtained from Kilburn and Petley (2003).

Houlsby et al. (2014) review some of the different data regarding input parameters to the Vajont slide. In table 1, table 2 and table 3, Houlsby et al. (2014: 801-802) data is summarised from different reports and investigations. The input parameters presented in table 1 below have been compared with the values presented by Houlsby et al. (2014) to verify the credibility of the data.

Input parameters	
Mass [kg]	6,4625E+11
g [m/s^2]	9,8
β [Radian]	0,64
Friction coefficient [-]	0,5
Length [m]	1200
Thickness [m]	240
Volume [m^3]	275 000 000
Specific weight [kN/m^3]	23,5
Max displacement [m]	240
Max velocity [m/s]	25

Table 1. Input parameters of Vajont slide.

3.1.2 Assumptions and applications

In order to simplify the calculation of the landslide, one solid block with triangular shape is assumed to be sliding down a slope. The geometry of the Vajont case is rather complex. Therefore, the geometry has been simplified according to figure 11. The alternative solution involves an analysis with two blocks and two interacting wedges, as discussed by Alonso (2010), and two different inclinations. The angle of the upper block would then be 37 degrees

and the other one horizontal. A two-block analysis involves more advanced equations and will therefore not be within the scope of this report.

The rock mass is assumed not to be deformable. To perform valid calculations, it would be troublesome to obtain satisfying results if the mass was deformable. If an assumption of a deformable mass would be considered it would require a FEM analysis such as the one performed in Crosta et al. (2016).

To analyse the shear strength and the effective stresses that the slope is exposed to the Mohr-Coulomb failure criterion is applicable. This implies the use of the Mohr-Coulomb theory, which was presented earlier in this report.

No block rotation is considered in the movement of the landslide, hence it is considered to be in moment equilibrium. This excludes any consideration of moment and 3D effects in the analysis presented.

3.1.3 Geometry of Vajont

The first model of the Vajont slide is based upon an updated geological model presented by Paronuzzi and Bolla (2012). There are various geological models and cross sections available, however, the one presented by Paronuzzi and Bolla (2012) is one of the more critical cross sections to be considered. The cross section in figure 10 presented below is a simplification of the Castelletto section of Mount Toc.

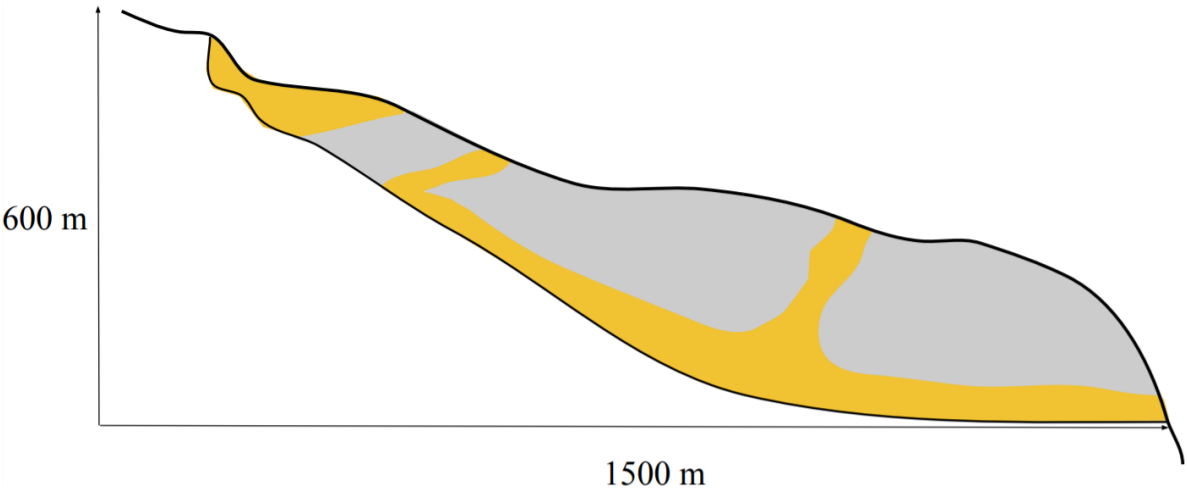

Figure 10. Castelletto section of Mount Toc. Author's own copyright.

3.1.4 Geometry and considered forces

In figure 11, the block has been simplified in order to facilitate analytical calculations. The inclination of the slope is marked as β and it has a value of 37 degrees according to Alonso et al. (2010). It could be reasonable to assume a mean value of the slope inclination, since one part of the sliding surface is horizontal and the upper block has an inclination of 37 degrees. However, a high slope inclination leads to a higher risk of slope failure. Therefore the slope inclination of 37 degrees is most suitable to consider.

The length of the landslide equals to 1700 m according to Müller (1987). Numbers for the height, based on Paronuzzi and Bolla (2012), equal 600 m for the landslide. Since both the length of the landslide and the height are known parameters, the upper length of the assumed geometry in figure 11 is calculated according to the Pythagorean theorem. This leads to a total length of 1500 m which is then divided into 1000 m and 500 m according to figure 11. The length is divided into 1000 m and 500 m to take into account the inclination of the rock mass. The upper surface is also lowered by 100 m in order to take the inclination of the geometry in figure 10 into account.

Relevant forces to be considered in this case are the weight of the rock mass which will be divided into driving and resisting force components, which is stated in kilonewton, as presented in figure 11. The normal force, *N*, is perpendicular to the sliding surface, whilst D, the driving force, is parallel to the sliding surface. The position of the forces has been decided on the basis of the centre of gravity of the sliding mass. The weight of the rock mass is illustrated as $W = m \cdot g$ in figure 11. In addition, a normal force, N, acts in the same but opposite direction of R. Between the sliding surface and the block a friction force appears, which is illustrated in figure 11, and is directed opposite to the driving force.

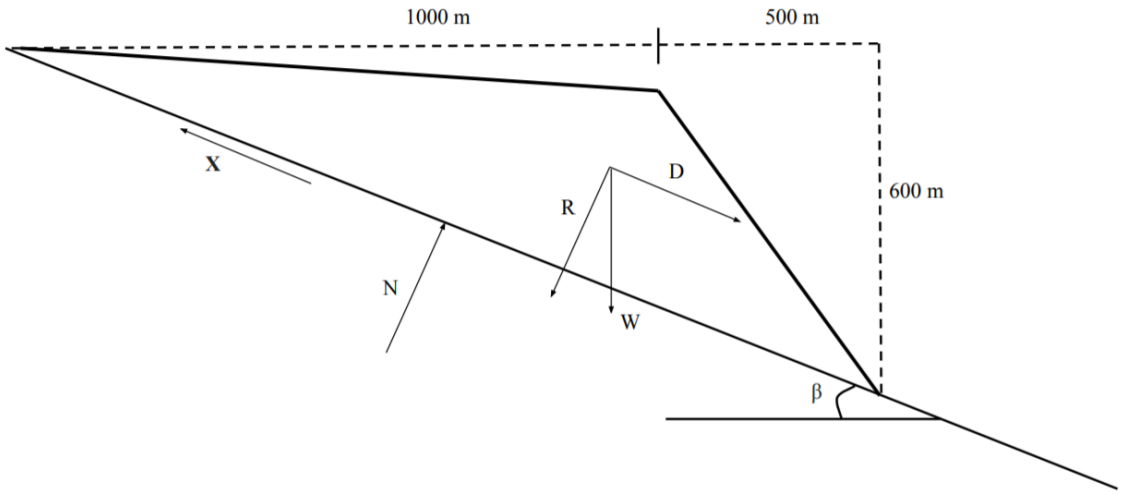

Figure 11. Simplified block geometry for mechanical sliding. Author's own copyright.

3.1.5 Performed calculations

For this case the calculations were firstly based on Newton's second law where $F = m \cdot a$, where *m* equals to the total mass [kg] of the landslide and a is the acceleration $[m/s^2]$.

F [N] is also defined as $F = D - R$, where D, is the driving force [N] and *R*, is the resisting force [N]. *D* is defined as $W \cdot sin(\beta)$ and R is given by $\mu \cdot W \cdot cos(\beta)$ according to Sällfors (2012).

Substituting the two equations above generates the following formula $m \cdot a = D - R$. By inserting the expressions for the driving and resisting forces the acceleration can be expressed as $a = g \cdot (sin(\beta) - \mu \cdot cos(\beta))$.

The factor of safety, *FS*, is then obtained by $FS = \frac{R}{D} = \frac{\mu \cdot W \cdot cos(\beta)}{W \cdot sin(\beta)}$. Hence the factor of safety only depends on the friction coefficient, weight of the sliding mass and the slope inclination. The effect of cohesion is therefore not considered in this case.

The acceleration can be calculated by assuming a friction coefficient of 0,5 which was found in Vajont clay, according to Kilburn & Petley (2003), and a slope inclination of 37 degrees. The acceleration is then considered to be constant since it only depends on the friction coefficient and the slope inclination. Acceleration can also be described as $a = \frac{\Delta V}{\Delta t} = \frac{V_2 - V_1}{t_1 - t_2}$. From this formula it is possible to obtain time values for different velocities ranging from 0 - 25 [m/s]. Finally, the displacements are expressed by $\Delta S = a \cdot t^2$, which are known at this stage. This makes it possible to plot the velocities versus the displacements of the landslide.

A sensitivity analysis was performed on the friction coefficient and the factor of safety regarding its impact on the acceleration. For the friction coefficient the values were altered between 0 - 1,2 in $FS = \frac{R}{D} = \frac{\mu \cdot W \cdot cos(\beta)}{W \cdot sin(\beta)}$, in the resisting force. Regarding the sensitivity analysis of the acceleration it was altered between values of $0 \leq \mu \leq 0{,}7$ of the friction coefficient in $a = g \cdot (sin(\beta) - \mu \cdot cos(\beta))$. The friction coefficient of approximately 0,7 indicates a factor of safety above 1.

3.2 Case 2 - Hydromechanical sliding

In contrast to the previous case this chapter will address how the presence of water in the reservoir affect the factor of safety. This case will therefore introduce additional forces such as uplift and hydrostatic water pressure forces induced by the water. The role of water impoundment and its impact on the factor of safety compared to the previous case will clarify the significance of the filling-drawdown of the reservoir.

Similarly to the previous case, the Mohr-Coulomb failure criterion, Newton's second law and trigonometric relations will be considered in the calculations. However, water induced forces will be applied in this case to emphasise the difference between both cases and the resulting impact on the factor of safety.

3.2.1 Input parameters

The input parameters for the case of hydromechanical sliding are the same as in the case of mechanical sliding. However in this case the new parameter will be the component angle of Q labeled as ε.

Input parameters	
Mass [kg/m]	646250000
g [m/s^2]	9,8
Slope inclination β [Radian]	0,65
Component angle of Q, ε [Radian]	0,23
Density of water [kg/m^3]	1000
Friction coefficient [-]	0,5
Volume of the slide mass [m^3]	275 000 000
Slip surface length, L [m]	1700
Specific weight [kN/m^3]	23,5
Max displacement [m]	240
Max velocity [m/s]	25

Table 2. Input parameters for case 2 - hydromechanical sliding.

3.2.2 Assumptions and applications

The forces considered in the landslide will be calculated per unit length. One of the reasons for this is because the analysis is in 2D and not in 3D. The cross-section is only valid for a limited width of the landslide. Therefore a width of 1 m is assumed in the calculations presented.

The mass is evaluated as $2350 \left[\frac{kg}{m^3}\right] \cdot 275\,000\,000\,m^3 = 6{,}4625 \cdot 10^{11}\,[kg]$ and is then converted into mass per unit length of the landslide by dividing the mass with the width of 1000 m. The evaluated mass can be found in table 2.

In order to calculate the uplift force and hydrostatic pressure, the sliding rock mass is assumed to be impermeable except in the sliding surface. In addition, no tension cracks will be considered in the analyses presented. Furthermore, the sliding surface and the clay underneath is considered to be fully saturated.

To sketch the geometry with the angles and water induced forces scalar paper has been used. This makes it possible to measure the distances connected to the uplift force and water pressure, see figure 13 for the corresponding lengths L_1 and L_2.

For the case of rapid drawdown, the uplift force is assumed to be constant and linked to the maximum elevation throughout the analysis independent of the drawdown of the water level.

When studying the relationship between the displacement, velocity and acceleration the timesteps will be constant. During the motion of the landslide the water will be raised in relation to the landslide mass. The end constraint for the analysis of the displacement, velocity and acceleration will be at the crest of the slope.

3.2.3 Geometry of Vajont

The figure below displays the same geometry as in figure 11 in the previous case. However, figure 12 below illustrates a water level in the reservoir. The water has not permeated the rock mass, but fully saturated the sliding surface.

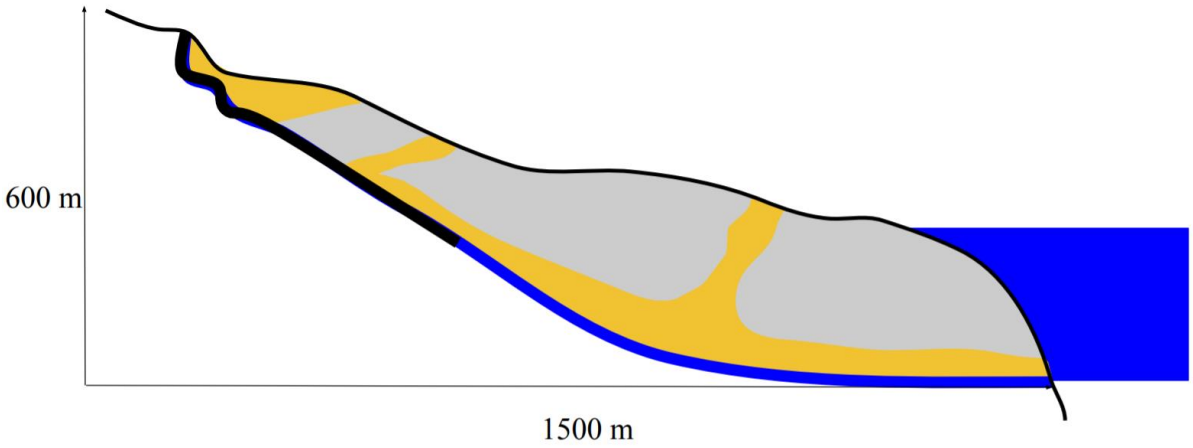

Figure 12. Castelletto section of Mount Toc with water in the reservoir. Author's own copyright.

3.2.4 Geometry and considered forces

In comparison to figure 12, figure 13 below is similar but with the addition of the uplifting force from the water, U, and the hydrostatic water pressure, Q. The hydrostatic water pressure is then divided into sine and cosine components of the angle, ε. This is in order to evaluate its components and its effect on the factor of safety.

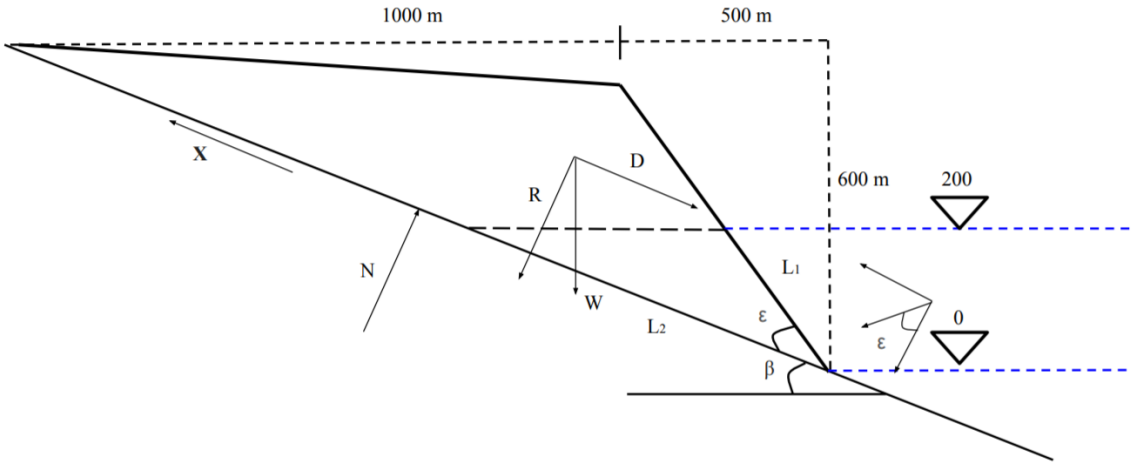

Figure 13. Simplified block geometry for the hydromechanical case. Author's own copyright.

Figure 14, below, illustrates the positioning of the block at different time-steps as the sliding of the block has been initiated. The water level is assumed to increase constantly in relation to the sliding of the block. As the block slides along the inclined plane, the water level changes in relation to the block. t_1 correspond to ΔS_1 and W_1, while t_2 correspond to ΔS_2 and W_2 and so on.

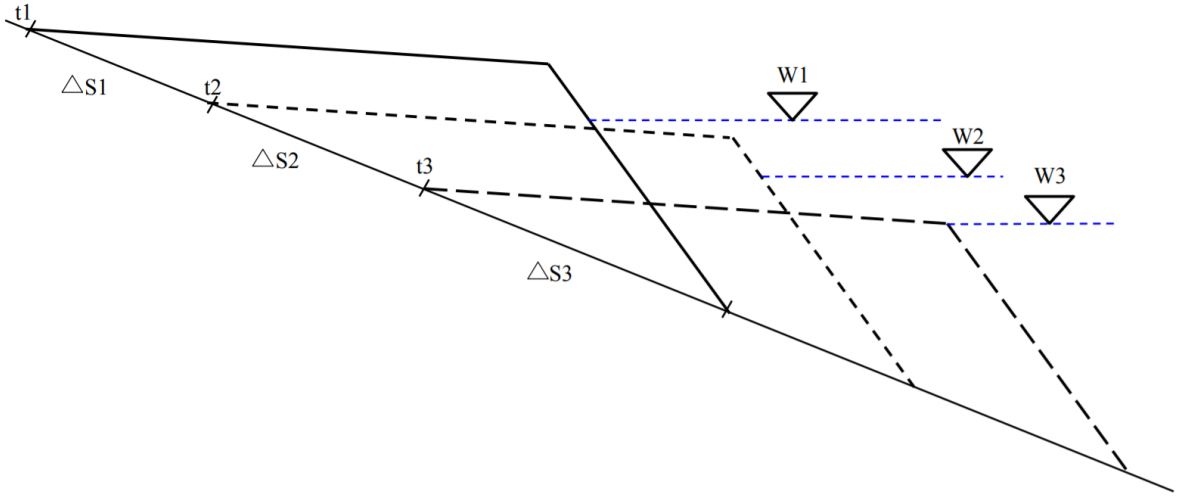

Figure 14. Simulation of the landslide at different time-steps with corresponding displacements and water elevations. Author's own copyright.

3.2.5 Performed calculations

Firstly, the hydrostatic water pressure, *P*, is considered to increase with depth according to $P = \rho \cdot g \cdot h_w$ $[Pa]$, where ρ equals to the density of water $[kg/m^3]$ and h_w is the water level in the reservoir.

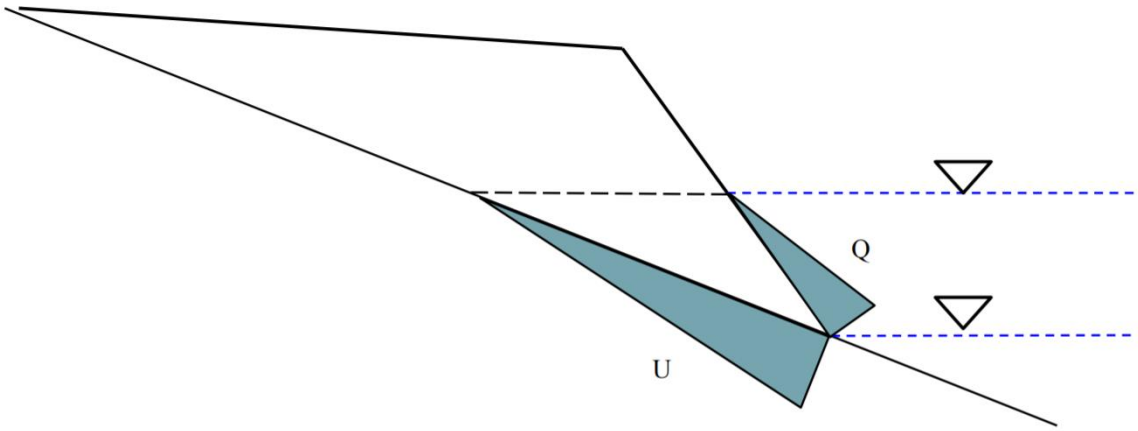

Figure 15. Illustration of the water pressure, Q and the uplift force U. Author's own copyright.

Therefore the water force will be evaluated as the area of the triangle, which is given by the following formulae: $Q = \frac{P \cdot L_1}{2}$ [N/m]. In figure 15, *Q* illustrates the force due to the water pressure, which increases linearly with depth.

Similarly to *Q*, the uplift force, *U*, is also considered to increase linearly with depth. However, U is distributed on the length of L_2 which belongs to the slip surface instead of acting on L_1 see figure 13.

Cohesion is evaluated by the formulae $cA = c \cdot 1 \cdot L$, where *L* is the length of the slip surface and 1 represent the width of the landslide, see table 10. The cohesive force, *cA*, is only

accounted for in calculations where the factor of safety exceeds 1, $FS \geq 1$. When the landslide is set in motion due to the factor of safety being lower than one, $FS \leq 1$, no cohesive force, *cA*, is exerted on the rock mass. The value of cohesion for the clay found in the slip surface of Vajont has been reported to be 762,3 kPa according to (Pinyol and Alonso, 2010).

The factor of safety for this case is evaluated as $F = \frac{R}{D} = \frac{(W \cdot cos(\beta) - U) \cdot tan(\varphi) + Q \cdot cos(\varepsilon) + cA}{W \cdot sin(\beta) - Q \cdot sin(\varepsilon)}$, this equation is based on the equilibrium of forces presented in figure 13, along with the consideration of the internal friction angle of the rock mass.

The angle of ε is calculated by trigonometric relations according to the following equation $\varepsilon = 90 - (\beta + arctan(\frac{500}{600})$. The purpose of determining the angle ε is to estimate the different components of the water force, *Q*, which is generated by the water pressure, *P*.

As illustrated in figure 14, the sliding block is assumed to exist in three different positions as the sliding has been initiated. This assumption makes it possible to calculate different velocities and accelerations. These are calculated for the three positions, which are labelled with index 1, 2 and 3. However more positions will be considered in the calculations but are not presented in figure 14 since it would make the figure unclear.

3.3 Case 3 - Thermomechanical sliding

The following case will provide better understanding how the variation in temperature affect the friction coefficient and by extension, also, affect the factor of safety. The Vajont slide was subjected to thermal softening. Therefore, the friction angle is assumed to decrease, as the temperature increases (Veveakis et al., 2007).

This chapter will employ the method of Veveakis et al. (2007) to investigate how the thermal softening process affects the frictional resistance force, ultimately increasing the total force of the landslide. One of the main mechanisms leading to the effect of the landslide, which increased the total force, was the acceleration. Therefore, this is an important issue to study in order to achieve a better understanding of the disaster.

3.3.1 Input parameters

The results of this case are based upon the following input parameters. μ_{res} is the residual friction coefficient, *N* is a frictional rate-sensitivity coefficient, *M* is a frictional thermal-sensitivity parameter and θ_1 is the reference temperature at a certain strain rate according to Veveakis et al. (2007). The slope inclination is, as mentioned previously, marked by $\beta = 37$ degrees.

Input parameters		
μres	0,18	Table2
N	0,01	Table2
M	0,01	Table2
Θ_1[C]	22,00	Table2
g [m/s^2]	9,80	-
β	37,00	-
Sin(β)	0,60	-
Cos(β)	0,80	-
Tan(β)	0,75	-

Table 3. Input parameters for the case of thermomechanical sliding. Table 2 is from Veveakis et al. (2007:12).

3.3.2 Assumptions and applications

To calculate the effects of thermal softening several assumptions have to be made to facilitate the calculations. The effect of diffusion will be neglected to simplify the calculation. This means that the temperature gradient will not be considered in the calculations.

In equilibrium the factor of safety equals to 1, $FS = 1$ and the friction coefficient, μ, equals to 0,754 as in the case of mechanical sliding. The reason for choosing this parameter is to make it possible for comparison between the cases. The starting temperature θ, will be equal to 0. In addition, the residual friction coefficient, μ_{res}, is assumed to be equal to the reference friction coefficient, μ_{res}= μ_{ref}, according to Veveakis et al. (2007). The shear strain rate has been evaluated with respect to these previous assumptions and is equal to 3,41.

The temperature is assumed to vary between $0\ °C \leq \theta \leq 160\ °C$. The upper limit has been chosen to emphasize the temperature effect on the factor of safety. Choosing the upper value $\theta = 160\ °C$ is large enough to capture the thermal effects on the factor of safety. Also, water effects will be neglected in this case. The focus will be to emphasize the temperature effects on the factor of safety.

3.3.3 Geometry and considered forces

The length and height of the block in figure 16 is assumed to be equivalent to the figure in the mechanical case, see figure 11. This assumption was made in order to facilitate cross-comparisons between the different cases in the method.

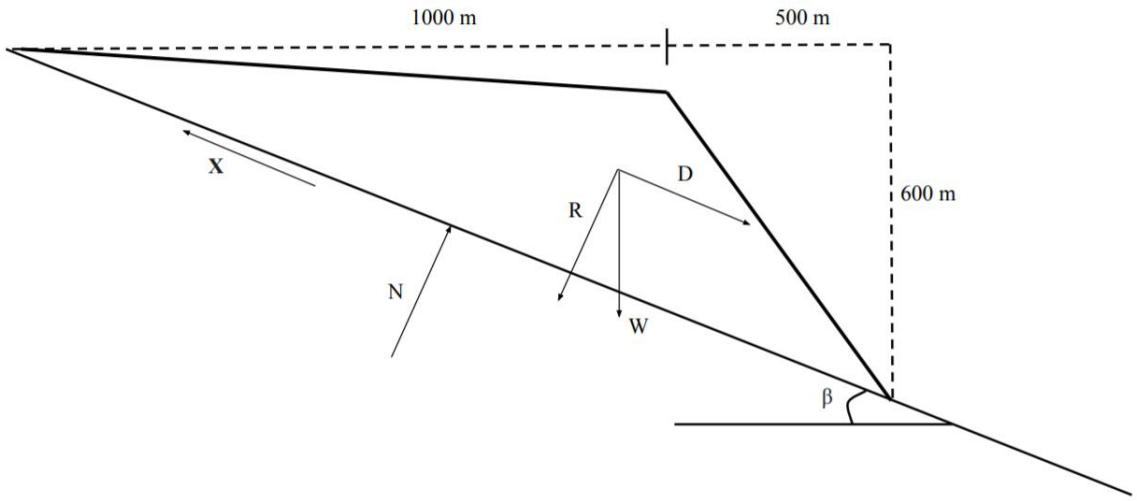

Figure 16. Simplified block geometry for the thermomechanical case. Author's own copyright.

3.3.4 Performed calculations

μ_{cs}, the critical state friction coefficient is defined by the following equation: $\mu_{cs} = \mu_{ref}(\frac{\dot{\gamma}}{\dot{\gamma}_{ref}})^N \cdot e^{-M(\theta-\theta_1)}$. According to Veveakis et al. (2007: 8) μ_{cs} has a constant value of 0,4 in the case of the Vajont slide. Furthermore, μ_{cs}, is assumed to be equal to μ_0. In these calculations thermal softening is assumed, which ultimately leads to the critical friction angle decreasing as the temperature increases. N and M are sensitivity parameters that are found in table 2 in Veveakis et al. (2007: 12). All variables with index *ref* are reference quantities (Veveakis et al., 2007). Every term in the equation below is constant except for the temperature θ, which will range between 0 ˚C and 160 ˚C. The purpose of the variation in temperature is to study how these variations affect the factor of safety. θ_1= 22 ˚C is the reference temperature according to table 2 in Veveakis et al. (2007: 12). The strain rate, change in deformation with respect to time, is defined by $(\frac{\dot{\gamma}}{\dot{\gamma}_{ref}})^N$and equals to 3,41 [-] in the following equation $\mu = \mu_0(\frac{\dot{\gamma}}{\dot{\gamma}_{ref}})^N \cdot e^{-M(\theta-\theta_1)} = \mu_{cs}$.

The obtained friction coefficient is used to calculate the acceleration, a $[m/s^2]$ according to $a = g(sin(\beta) - \mu(cos(\beta))$. The variation in friction coefficient lead to different values of acceleration and resisting force. The lower the resisting force the higher the acceleration will become. Therefore, the degree of acceleration determines the size of the total force. This means that the total force will increase since $D - R = m \cdot a$. Hence, the decrease in factor of safety increases the acceleration, which leads to a higher risk of failure meaning that the equilibrium state is surpassed.

A high acceleration generates a higher velocity, $a = \frac{\Delta V}{\Delta t}$, determined by the defined timesteps provided for the calculation. In this case the time is assumed to vary between $5\ s \leq t \leq 12{,}6\ s$. The reason for limiting the interval to the lower and upper limit of is to make it easier to compare it with the mechanical case, see table 6 for the time steps used in the mechanical case. The distance covered by the landslide, displacement *S* [m] is then calculated by $\Delta S = a \cdot t^2$.

As a conclusion when different values of the friction coefficient are obtained the factor of safety can be evaluated according to the following formulae, similar to the mechanical case:

$$FS = \frac{\mu \cdot mg \cdot cos(\beta)}{A} \cdot \frac{A}{mg \cdot sin(\beta)} = \frac{\mu}{tan(\beta)}$$

The performed calculations all generate different graphs. These include the friction coefficient vs. temperature, temperature vs. acceleration, factor of safety vs. temperature, velocity vs. temperature and velocity vs. displacement.

4. Results

The former chapter presented the analysis of the Vajont slide by mechanical, hydromechanical and thermomechanical methods. In the upcoming chapter tables and graphs will be presented to the three cases. Also, a sensitivity analysis of the input parameters will be conducted for all the cases. This analysis is important to better understand how the different parameters influence each other.

4.1 Case 1 - Mechanical sliding

As a starting point for the analysis, static equilibrium is assumed when the factor of safety equals to 1, $FS = 1$. This leads to the friction coefficient having a value of 0,754 according to the table 4.

Calculations	
Driving Force [kN]	3811444995
Resisting Force [kN]	3813700591
FS	1,00
Equilibrium at friction coefficient 0,754	

Table 4. The driving, resisting and resultant forces along with the factor of safety and failure criterion.

A first sensitivity analysis is presented in figure 17, where the factor of safety, *FS* is plotted against the friction coefficient. The figure shows that when the friction coefficient is lower than 0,754 the equilibrium state is lost. After this point, the risk of failure increases remarkably. This is due to the factor of safety being lower than, *FS* < 1.

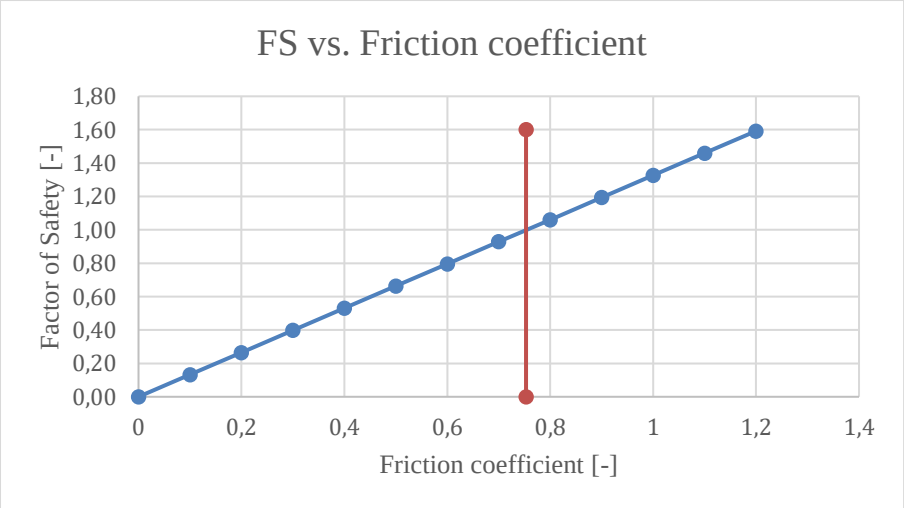

Figure 17. Factor of safety vs. Friction coefficient. Author's own copyright.

For the second sensitivity analysis values for the acceleration is evaluated when the equilibrium state is lost. At this point the factor of safety is below 1, *FS* < 1 as indicated in table 5.

Acceleration	FS	Friction coefficient
-	1,59	1,2
-	1,46	1,1
-	1,33	1
-	1,19	0,9
-	1,06	0,8
0,42	0,93	0,7
1,20	0,80	0,6
1,98	0,66	0,5
2,77	0,53	0,4
3,55	0,40	0,3
4,33	0,27	0,2
5,12	0,13	0,1
5,90	0,00	0

Table 5. The relationship between acceleration, factor of safety and friction coefficient.

The following graph was plotted in figure 18 to illustrate the relation between the factor of safety and acceleration. As expected, the decrease in the factor of safety leads to a remarkable increase in acceleration. Furthermore, this also increases the velocity and displacement of the landslide.

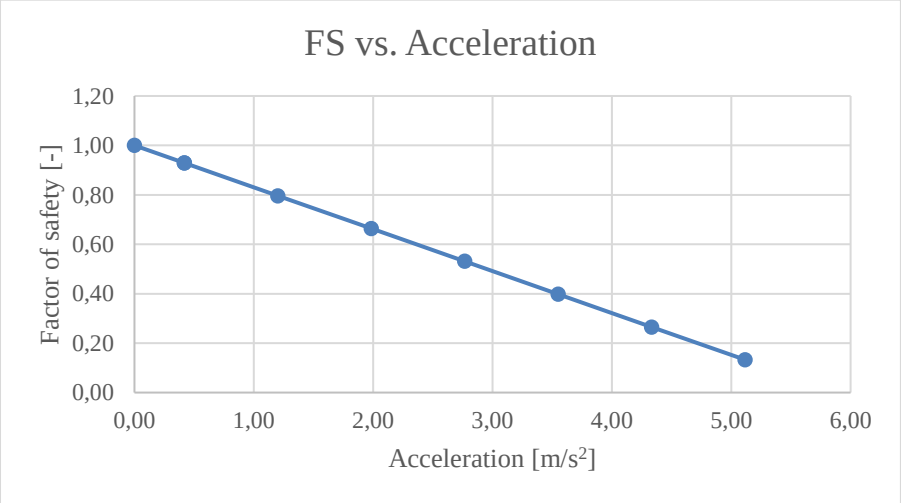

Figure 18. Factor of Safety vs. Acceleration. Author's own copyright.

According to Kilburn & Petley (2003) the friction coefficient equals to 0,5 for the clay found in the sliding surface of Vajont. From the equation $a = g(sin(\beta) - \mu \cdot cos(\beta))$ a constant acceleration is obtained at 1,98 $[m/s^2]$. Different time values are calculated based on varying the velocity, on an interval of $0 \leq V \leq 25$ $[m/s]$. Accordingly, the displacement will be evaluated and presented in the table 6.

Time [s]	Velocities [m/s]	Displacement [m]
12,6	25	314,95
10,1	20	201,56
7,6	15	113,38
5,0	10	50,39
2,5	5	12,60
0,0	0	0,00

Table 6. Relationship between different times, velocities and displacements.

As a conclusion the velocities and displacements in table 6 is plotted in figure 19. The orange line at the displacement of 240 m marks the maximum allowed sliding distance which was justified by Müller (1987).

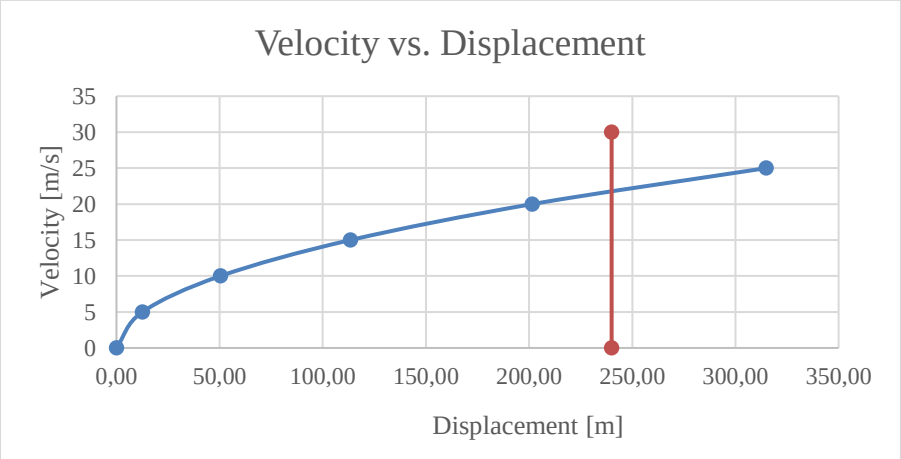

Figure 19. Velocity vs. Displacement. Author's own copyright.

4.2 Case 2 - Hydromechanical sliding

The hydrostatic water pressure, P, was evaluated at five different depths ranging between $0\,m \leq h_w \leq 200\,m$, see table 7. As expected, the hydrostatic water pressure increases with increasing depth.

Water depth [m]	P, Hydrostatic water pressure [kPa]
200	1960
150	1470
100	980
50	490
0	0

Table 7. Hydrostatic water pressure in relation to water depth.

The water force Q is calculated in relation to the different lengths, represented by $L_1$and water depths presented in table 8.

Water depth [m]	Length, L1 [m]	Q, Water force [kN/m]
200	250	245000
150	190	139650
100	130	63700
50	70	17150
0	0	0

Table 8. Correlation between water depth, length, L_1, and water force.

Similarly to the water force the uplift force, U, is then evaluated in relation to the lengths, represented by L_2 and water depths presented in table 9.

Water depth [m]	Length, L2 [m]	U, Uplift force [kN/m]
200	420	411600
150	310	227850
100	210	102900
50	100	24500
0	0	0

Table 9. Correlation between water depth, length (L2) and uplift force.

For the case of a friction angle of 40 degrees, moment equilibrium is not obtained and therefore the effect of cohesion must be applied to the resisting force according to table 10.

Cohesive fore [kPa]	(cA) = L * c * width [kN/m]
762,3	1295910

Table 10. The cohesive force considered.

Then the water force, *Q*, is divided into components according to table 11. See figure 13 for details regarding the considered forces.

Component water forces [kN/m]			
Water depth [m]	Q	Q * SIN(ε) (Driving force)	Q * COS(ε) (Resisting force)
200	245000	55113	238721
150	139650	31414	136071
100	63700	14329	62067
50	17150	3858	16710
0	0	0	0

Table 11. Component water forces in relation to water depth.

4.2.1 Study of the equilibrium forces

In figure 20 the factor of safety is plotted as a function of the elevation of water in the reservoir. Here the friction angle, φ, equals to 40 degrees. As the elevation of water increases, the factor of safety decreases. This is due to the effect of the hydrostatic pressure and the uplift force.

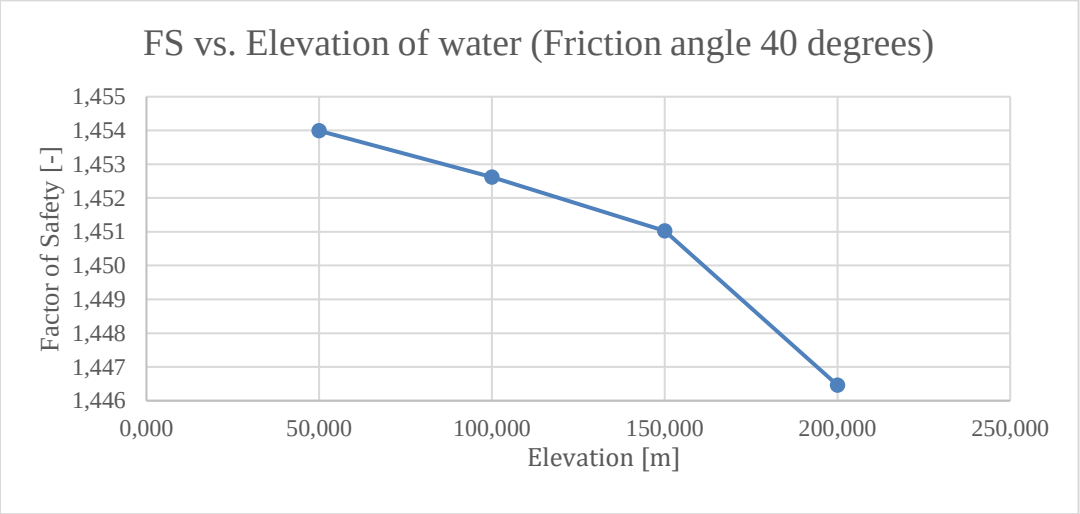

Figure 20. Factor of Safety vs. elevation of the reservoir for a friction angle of 40 degrees. Author's own copyright.

Compared to the figure above, figure 21 has assumed a friction angle φ of 30 degrees. In this case, the factor of safety increases as the elevation of water increases. Despite the effect of water pressure and uplift force the factor of safety increases. This is due to the change in friction angle.

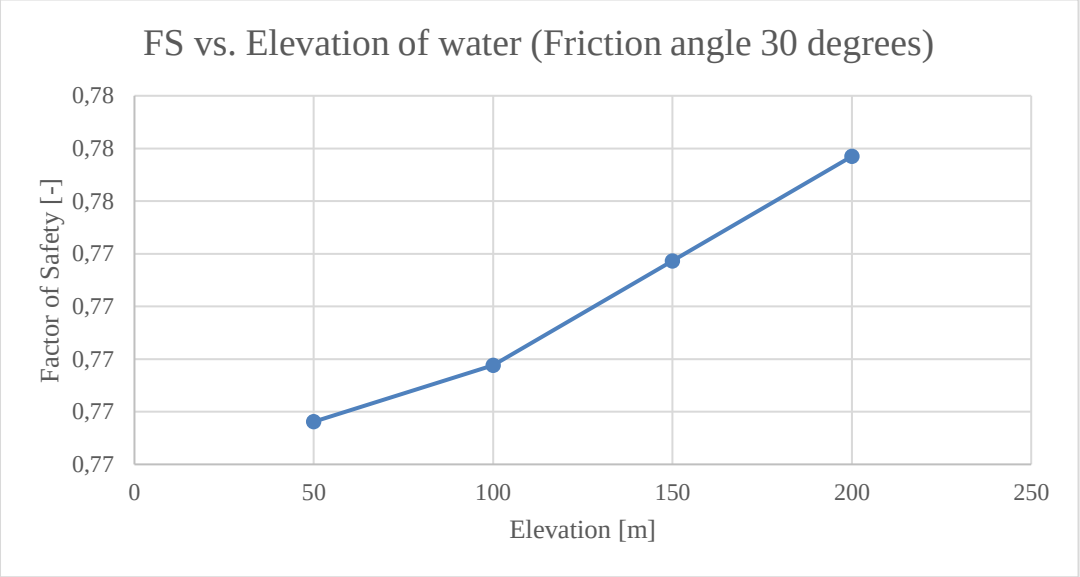

Figure 21. Factor of Safety vs. elevation of the reservoir for a friction angle of 30 degrees. Author's own copyright.

The figure 22 shows a similarity between this figure and the figure above. The only factor that differs is the friction angle, however, the distribution of hydrostatic pressure and the uplift force is the same in both cases. Therefore, they should be similar.

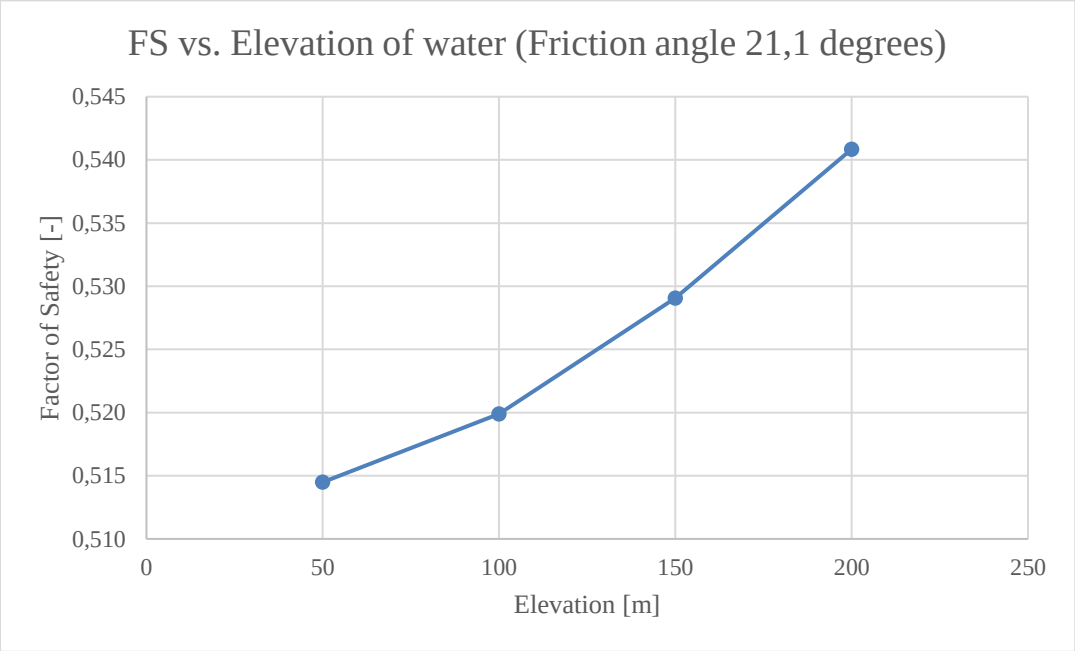

Figure 22. Factor of Safety vs. elevation of the reservoir for a friction angle of 21,1 degrees. Author's own copyright.

4.2.2 Fast drawdown

For the case of fast drawdown, the uplift force, *U*, is set to 200 m being the maximum elevation of the reservoir as mentioned previously in the assumptions and applications.

In figure 23 the factor of safety is based on the elevation of the reservoir, for a friction angle of 40 degrees. As can be seen in figure 23, the factor of safety decrease as the elevation decreases.

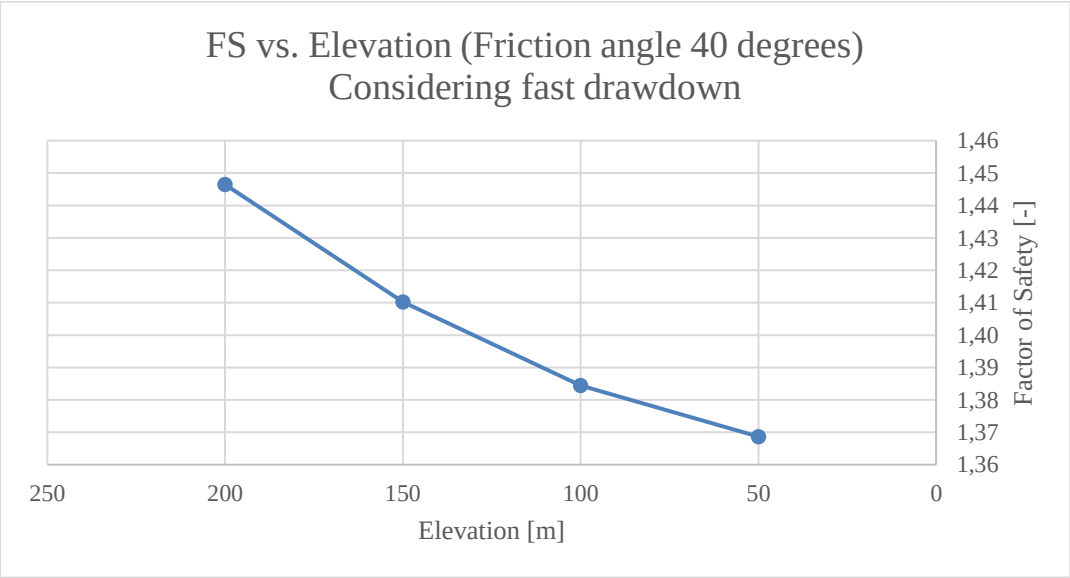

Figure 23. The impact of fast drawdown on the Factor of Safety vs. elevation of the reservoir for a friction angle of 40 degrees. Author's own copyright.

Figure 24 displays the same relation as in figure 23. The only differing factor is the friction angle, which is 30 degrees in figure 24.

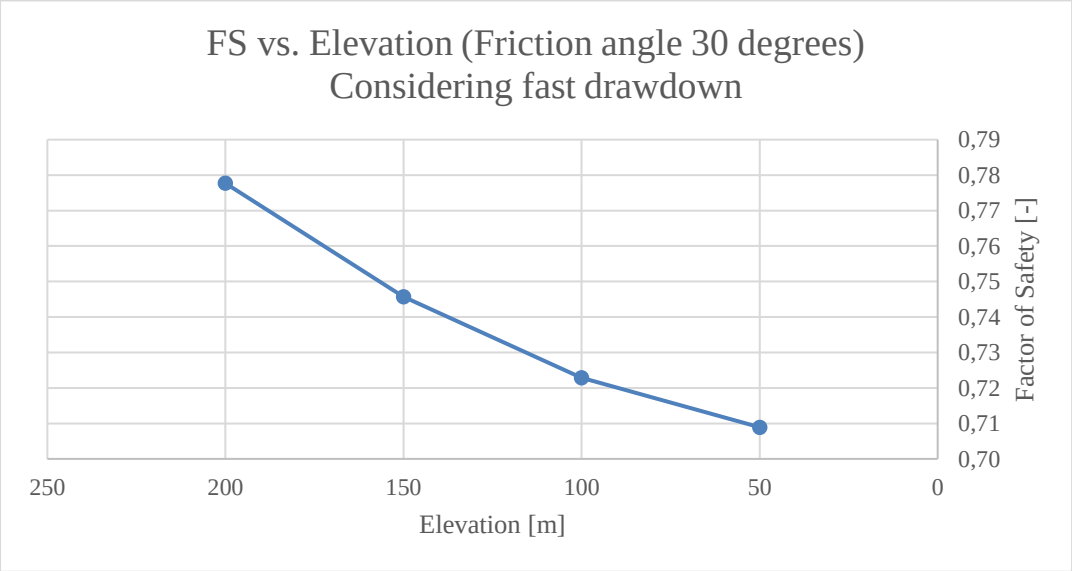

Figure 24. Fast drawdown and its impact on the Factor of Safety vs. elevation of the reservoir for a friction angle of 30 degrees. Author's own copyright.

Figure 25 illustrates the same relation as figure 23 and figure 24. However, here the friction angle is reduced to 21,1 degrees. The graph in figure 23, figure 24 and figure 25 all behave similarly and the factor of safety decreases as the elevation increases.

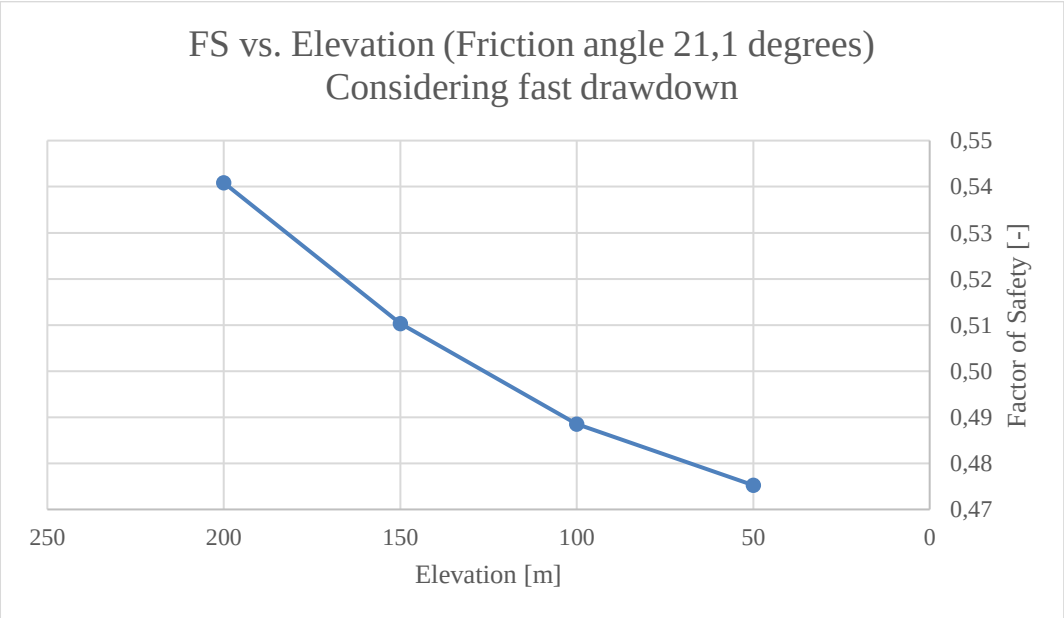

Figure 25. Fast drawdown and its impact on the Factor of Safety vs. elevation of the reservoir for a friction angle of 21,1 degrees. Author's own copyright.

4.2.3 Velocity vs. displacement of the landslide

Table 12 illustrates how the hydrostatic water pressure increases when the water depth increases for elevations ranging between $300\ m \leq h_w \leq 500\ m$.

Water depth [m]	P, Hydrostatic water pressure [kPa]
500	4900
400	3920
300	2940

Table 12. The input hydrostatic water pressure, P, for the case of fast drawdown.

Water force, Q, in table 13 is distributed as a triangle perpendicular to the surface of the landslide that is covered by water. Table 13 shows this value in relation to length, L_1, and water depth.

Water depth [m]	Length, L1 [m]	Q, Water force [kN/m]
500	550	1347500
400	460	901600
300	360	529200

Table 13. The input water force, Q, for the case of fast drawdown.

Table 14 include the value of the uplift force in relation to length, L_2, and water depth.

Water depth [m]	Length, L2 [m]	U, Uplift force [kN/m]
500	1050	2572500
400	840	1646400
300	630	926100

Table 14. The input uplift force, U, with corresponding lengths and elevation of the reservoir for the case of fast drawdown.

In table 15 the water force, Q, has been divided into component forces that affect the resisting and driving forces of the landslide.

Component water forces [kN/m]			
Water depth [m]	Q, Water force	Q * SIN(ε) (Driving force)	Q * COS(ε) (Resisting force)
500	1347500	303122	1312964
400	901600	202816	878492
300	529200	119044	515637

Table 15. The input components of the water force, Q, with corresponding elevations for the reservoir for the case of fast drawdown.

As illustrated in figure 26, the velocity is plotted as a function of the displacement for an interval between $200\,m \leq h_w \leq 500\,m$. The values of the water depth elevation presented above are only three points that have been taken into consideration. However, the remaining values were also calculated in 25 m intervals between the values presented of the water elevation in table 12, 13, 14 and 15. This is in order to obtain an accurate graph in figure 26 and 27.

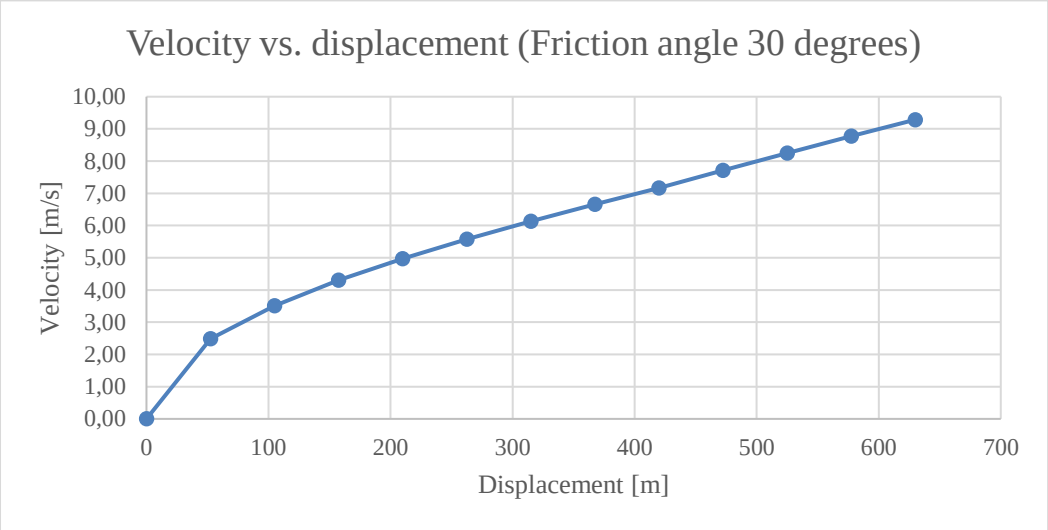

Figure 26. Velocity vs. displacement for a friction angle of 30 degrees. Author's own copyright.

In figure 27 as the displacement increases, the velocity increases similarly to the previous case. The difference between figure 27 compared to figure 26 is that velocity increase in a faster rate in relation to the displacement in figure 27. This is a result of the difference in the value for the friction angle.

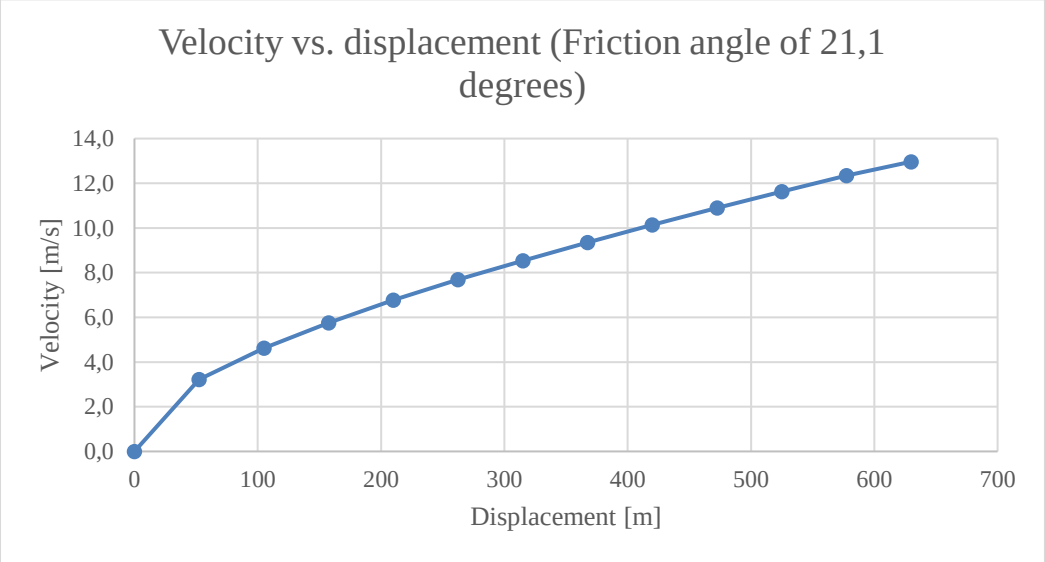

Figure 27. Velocity vs. displacement for a friction angle of 21,1 degrees. Author's own copyright.

4.3 Case 3 - Thermomechanical sliding

Table 16 demonstrate how different values for the temperature, θ, generate different values of the friction coefficient. The increase in θ leads to a decrease in the friction coefficient. The evaluated friction coefficient in table 16 can also be found in table 17 to further explain the correlation between the friction coefficient and the different parameters.

θ	θ1	$e^{-M(\theta-\theta_1)}$	$(\frac{\dot{\gamma}}{\dot{\gamma}_{ref}})^N$	μ
0,00	22,00	1,23	3,41	0,75
20,00	22,00	1,02	3,41	0,63
40,00	22,00	0,85	3,41	0,52
60,00	22,00	0,70	3,41	0,43
80,00	22,00	0,58	3,41	0,36
100,00	22,00	0,48	3,41	0,30
120,00	22,00	0,40	3,41	0,25
140,00	22,00	0,33	3,41	0,20
160,00	22,00	0,28	3,41	0,17

Table 16. Temperature variation effects on the friction coefficient according to equation (2).

Table 17 shows that the equilibrium state is obtained when the factor of safety equals to 1, this is achieved when the friction coefficient = 0,75. Table 17 also shows how the μ decreases as the acceleration increase. The variation in time between $5\ s \leq t \leq 12{,}6\ s$ generate different values of velocity, which enables the calculation of the displacement in the same table.

μ	a	FOS	t	V	S
0,75	0,00	1,00	5	0,00	0
0,63	1,00	0,83	6	6,01	36
0,52	1,83	0,69	7,6	13,92	106
0,43	2,52	0,57	8	20,18	161
0,36	3,10	0,48	9	27,86	251
0,30	3,57	0,39	10,1	36,07	364
0,25	3,97	0,33	11	43,62	480
0,20	4,29	0,27	12	51,52	618
0,17	4,57	0,23	12,6	57,53	725

Table 17. Friction coefficient and its impact on Factor of Safety, velocity and acceleration.

The graph in figure 28 describes the correlation between the friction coefficient and the temperature of the landslide according to the values obtained in table 16.

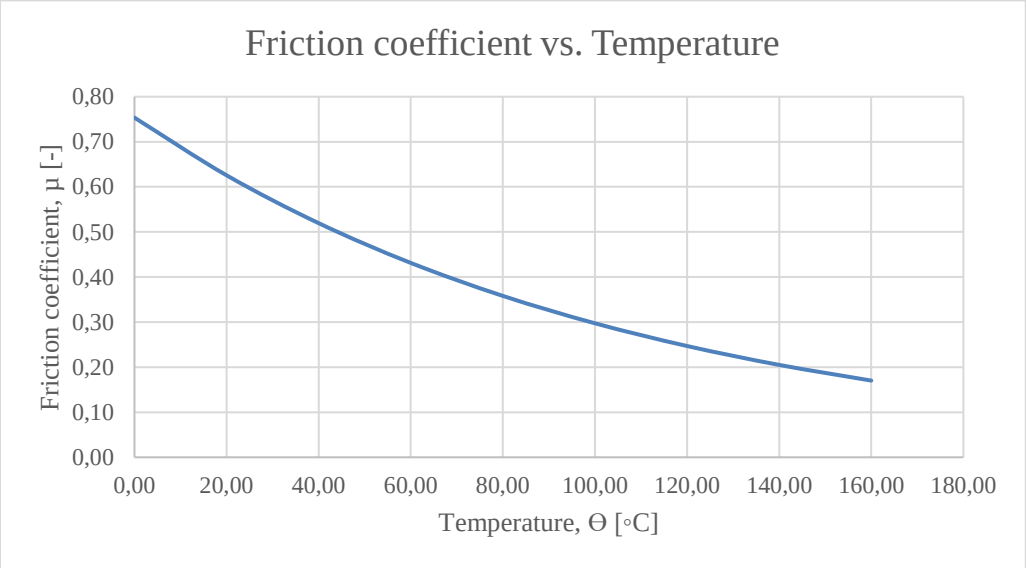

Figure 28. Friction coefficient vs. Temperature. Author's own copyright.

Figure 29 illustrates the relation between acceleration and temperature of the landslide. As the acceleration increase the temperature follows a slightly positive exponential curve.

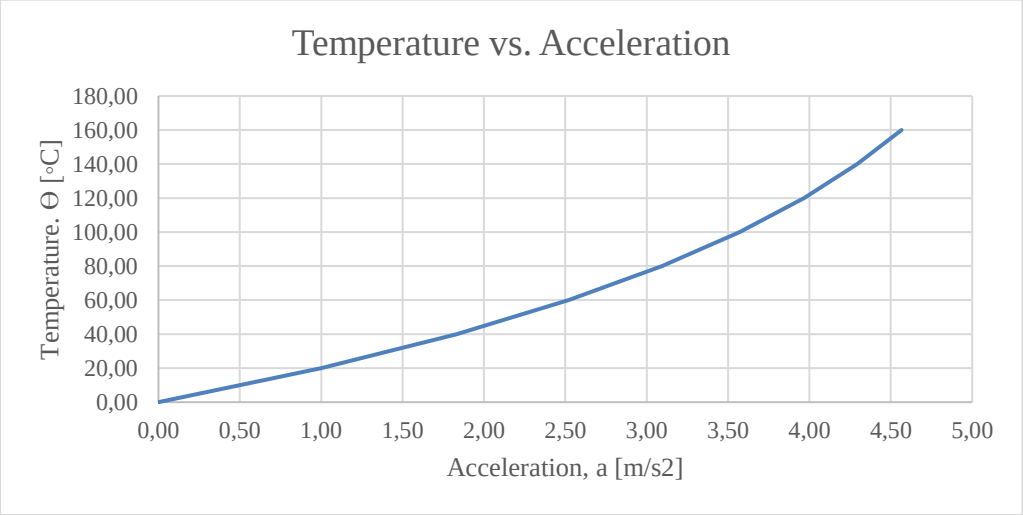

Figure 29. Temperature vs. Acceleration. Author's own copyright.

In figure 30 the relation between velocity and temperature of the landslide is shown. The temperature increases linearly as the velocity increases.

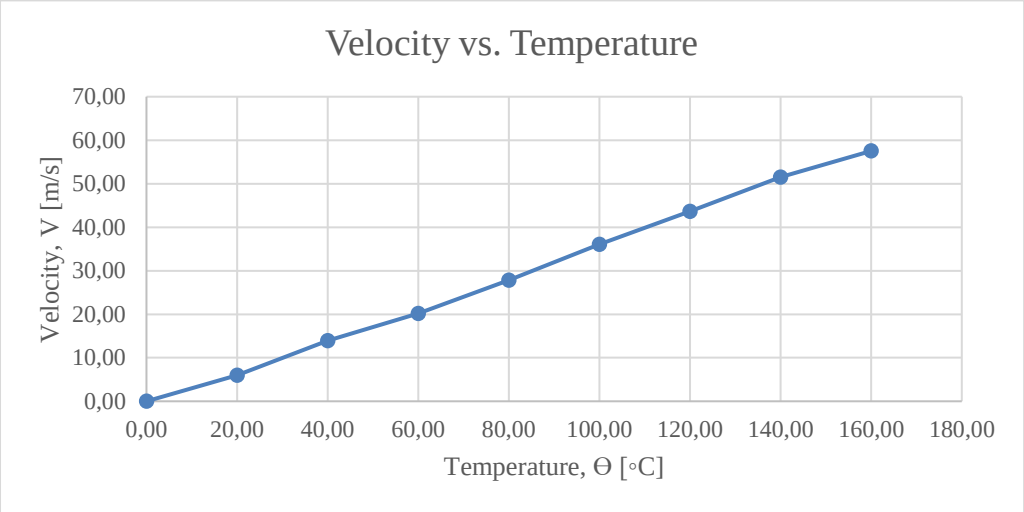

Figure 30. Velocity vs. Temperature. Author's own copyright.

Figure 31 shows the link between factor of safety and the temperature of the landslide. As can be seen in figure 31 the factor of safety decreases as the temperature increases. Hence, the factor of safety is sensitive to high temperatures.

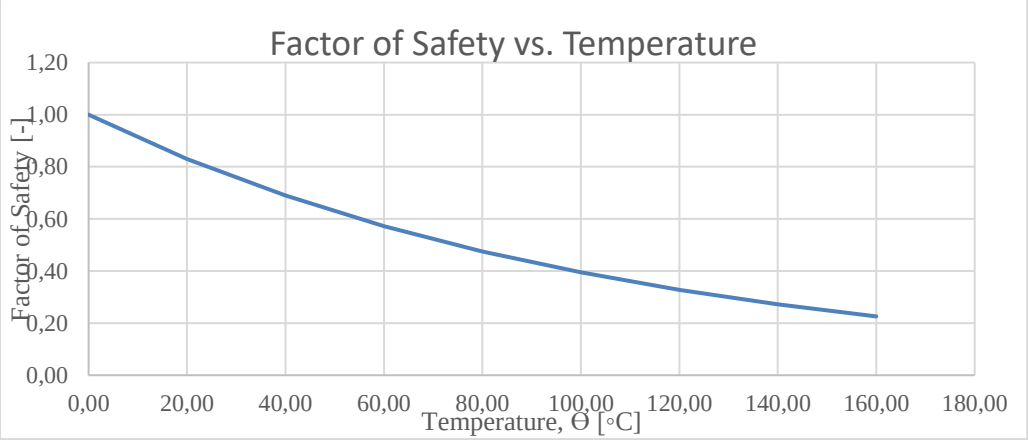

Figure 31. Factor of Safety vs. Temperature. Author's own copyright.

As can be seen in figure 32, the displacement increases for higher velocities.

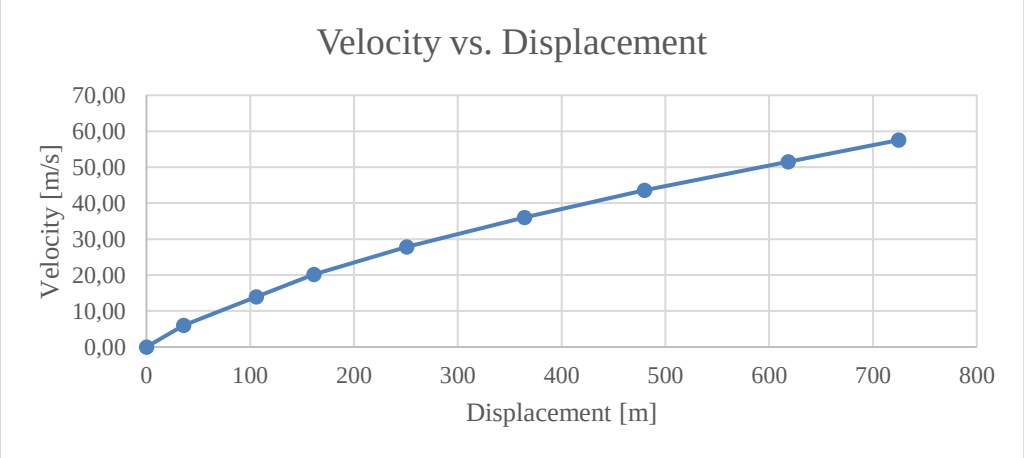

Figure 32. Velocity vs. displacement. Author's own copyright.

5. Discussion

This chapter will firstly treat a case comparison between the three cases presented in the method and results. Aspects such as effects on the factor of safety and the relationship between velocity and acceleration will be discussed. A discussion regarding the mitigations, modern standards and a line of action to avoid the Vajont slide will also be presented. Finally, several recommendations for further studies will be presented.

5.1 Case comparison

The three different cases share similar results regarding the factor of safety and velocity vs displacement. However, there are also some differences between the cases which will be presented in this chapter along with a discussion about the suitability of the studies presented. Suggestions for further research will also be addressed.

5.1.1 Factor of safety

For the mechanical and thermomechanical case of sliding the evaluated factor of safety for the two cases can easily be compared. This is since both cases are based on similar equilibrium equations for the factor of safety and pore-pressure effects are excluded in the thermomechanical case. The result of both cases is that the acceleration increases with a decreasing factor of safety, see figure 18 and table 17 for details. This is an expected behaviour since the acceleration is reduced by an increase of the friction coefficient in $a = g \cdot (sin(\beta) - \mu \cdot cos(\beta))$. The factor of safety is also based on the same equation $FS = \frac{\mu \cdot mg \cdot cos(\beta)}{A} \cdot \frac{A}{mg \cdot sin(\beta)} = \frac{\mu}{tan(\beta)}$ for both cases.

However, in the thermomechanical case the shear strain rate could alternatively have been evaluated according to $\dot{\gamma} = \frac{v_{max}}{2e}$ in order to obtain variations of the shear strain rate in relation to depth. This would render a different type of result compared to the assumption of the shear strain rate presented in the method for the thermomechanical case. Furthermore, the starting temperature was assumed to be at 0 degrees. It might have been more applicable to assume a temperature that somewhat corresponds to the actual mean air temperature of Vajont as an initial value.

In the case of hydromechanical sliding the factor of safety depends on a number of additional forces as presented in the method and results. Therefore, a comparison between this case and the mechanical and thermomechanical case is not very applicable. For the case of studying the equilibrium forces the factor of safety decreases with increasing elevation for a friction angle of 40 degrees, see figure 20. In the case of a friction angle of 30 and 21,1 degrees the factor of safety increases with respect to raising the reservoir level, see figure 21 and 22. One of the possible reasons for this phenomenon was considered to be the effect of cohesion added in the case of a friction angle of 40 degrees, along with the landslide being in equilibrium state with a factor of safety initially being above one. Furthermore, when the elevation of the reservoir is at the maximum water level of 200 m the uplift force, U, is significantly larger than the

component water force, Q. These three effects contribute to the factor of safety decreasing with increasing of the water level in figure 20.

When considering the case of fast drawdown for the three different friction angles the factor of safety was lowered quite remarkably for all cases, see figure 23, 24 and 25 for details. This is in line with the theory section that described the effect of rapid drawdown on slope stability. As mentioned in the rapid drawdown chapter a decreasing water table reduces the supporting water load, hence lowering the factor of safety. There was also a discussion in the chapter of rapid drawdown regarding a pore-pressure delay when lowering the reservoir affecting the uplift force, U. Since the uplift force is set to be constant at an elevation of 200 m despite the lowering of the water table the results can be considered reasonable.

The most important assumption that affects the factor of safety was concluded to be the inclination of the slope. This is because it plays a key role in almost all the cases that were studied. A higher slope inclination increases the driving force and reduces the resisting force significantly. It also plays a huge part in most of the equilibrium equations involved for all the cases.

5.1.2 Velocity vs. displacement

Similarly, to the comparison of the factor of safety for the three cases the mechanical and thermomechanical sliding share similar results regarding the velocity vs. displacement. In figure 19 and figure 32 it is evident that the increase of velocity vs. displacement follows a similar curve. However, in the case of thermomechanical sliding the increase of the velocity is faster compared to the mechanical case. This is due to thermal softening taking place.

The case of hydromechanical sliding also follows a similar curve which is expected. However, the interval of the velocities are significantly lower than for the other two cases. The introduction of a hydrostatic water pressure leads to a higher resisting force which by itself lowers the acceleration. Hence the results can be considered logical.

The maximum velocity of 25 $[m/s]$ suggested by Müller compares well to the results from the mechanical and thermomechanical case of sliding, see figure 19 and figure 32. This is likely due to most of the input parameters being gathered from Müller for the two cases. However, for the hydromechanical case the maximum velocities at a displacement of 240 $[m]$ were around 6 $[m/s]$, see figure 26 and figure 27. This is likely due to the individuality of the case of hydromechanical sliding since it considers the effect of water. Figure 13 illustrates how the water level in the reservoir counteracts the driving force. This leads to lower velocities compared to the other two cases hence the results are reasonable.

5.2 Suitability and further studies

The amount of simplifications and assumptions in the methods presented in this report makes the results kind of challenging to compare with previous research of the Vajont slide. However, these simplifications and assumptions were necessary in order to limit the scope of this thesis.

Despite the vast of number of assumptions and simplifications presented in this paper the results share similarities to the real case of the Vajont slide. For example, the effect of rapid drawdown drastically lowers the factor of safety, as presented in the theory part. Furthermore, the effect of thermal softening reduces the factor of safety in line with the theory part.

Further studies are required regarding the effect of seepage, tension cracks, orientation of cracks, amount of precipitation and multiphysical coupling. These studies are also relevant to be taken into consideration to understand all the mechanisms acting on the landslide and how they interact. The complexity of considering all these parameters requires the need for computer simulations which were not considered to be within the scope of this thesis.

5.3 Mitigations and modern standards

If the Vajont dam was constructed today the entire project and process would have been organised differently. The economic and political situation in Italy is significantly different today compared to when the Vajont dam was built. In addition, modern standards could enable better decision-making since these techniques are able to provide a larger picture of the risk of Vajont and, perhaps, even preventing the landslide from happening.

Even though investigations were carried through, these were not sufficient. Modern standard techniques could have provided more information about the landslide, its geometry and the scale of it, prior to the disaster. Computer programs were not invented at the time, therefore the simulations and the data processing techniques were not available during this era. The results from these techniques could have provided information that would have been helpful in mitigating the consequences of the landslide and, hopefully, urged for a more immediate and extensive evacuation of the villages.

The study of passive seismic earth movement by reservoir monitoring could perhaps have generated more information about the movement of the mountain. This sort of monitoring could have provided information on how the filling and lowering of the reservoir level affected the landslide. The wave that was produced from the landslide could have been predicted with flow-slide propagation. However, to do this information regarding the magnitude of the landslide would have had to be known.

Close-range photogrammetry, CRP, is not as useful as other ground-based monitoring techniques. CRP only examines the landslide and is mostly used for tracking and comparisons of surfaces. However, fixed terrestrial photogrammetric system is another monitoring technique where sensors are installed in the rock mass. This system allows for better information regarding the movement of the mountain and the behaviour of the landslide itself. The sensors could, for example, indicate that the rapid drawdown of the reservoir generated extensive movement of the sliding mass, if this was the case.

Remote-sensoring techniques could have been useful to monitor smaller rockfalls before the disaster took place. This technique could have contributed with information on the position of the main joints of the landslide, which would have explained the extensiveness of the landslide. To understand the landslide even better, terrestrial laser scanning could have analysed the geometrical properties of the landslide. This sort of data is difficult to collect in any other way due to the difficult terrain.

In summary, there are various new methods that were not available at the time of Vajont. As a result, these present-day methods have raised standards regarding planning and execution of large-scale geotechnical projects. All of these techniques are important to better predict the risk of landslides in general. However, there were investigations carried through and monitoring was conducted even though this research did not correspond to modern standards of today. The output from these investigations, however, sometimes disregarded if the indications were unfavourable for the project.

5.4 Line of actions to avoid the disaster

Renowned researchers in the field of geotechnics and rock mechanics propose several suggestions on the line of actions that might have prevented the landslide. From the theory and cases presented in the report along with the literature and research provided, this is the concluded line of action that could have been taken into consideration:

- *The water level should not have been raised to such an extent*. There should have been a margin of safety for the maximum water elevation in place based on site investigations.
- *The capacity of the drainage tunnels should have been increased*. It is important to have emergency solutions in place for unpredictable occasions where immediate actions are required.
- *An emergency reservoir connected to the main reservoir*. This would reduce the pressure, if needed, in the main reservoir.
- *The velocity of water impoundment should have been reduced*. This is because the case of rapid drawdown is highly critical from the conclusions of this report.
- *Evacuate the area after observing the warning signs*. For example, the 2 km crack should have been taken more seriously.

5.5 Role of ethics

The Vajont slide can be regarded as a geotechnical disaster and often is. However, there are many layers to the catastrophe and these are not purely geotechnical. Any infrastructure ultimately leads to the alteration of both the non-human and the human environment. To alter the environment means change for the entire ecosystem and the outcome of change is not predictable and, therefore, there is risk attached to it. This adds an ethical dimension to any engineering project as these decisions affect entire ecosystems. Whether something is ethical or unethical is difficult to pinpoint and often intuitive. However, there are laws that try to account for this. To better pinpoint the concept of ethics, it is reasonable to argue that it is unethical to execute any orders that provide little guarantee for the safety of many people's

lives. Moreover, to construct any infrastructure engineers must make assumptions regarding the project site. It is difficult to identify all characteristics, as well as recognising the consequences of multi-physical coupling. However, this does not imply that monitoring and research is needless, but quite the opposite. Therefore, many assumptions have to be made in the planning process and most of these assumptions carry with them some sort of risk. By these terms the Vajont is no different from any other hydraulic construction. Although there is a difference between making justifiable assumptions and neglecting negative indications, only to make new assumptions that are aligned with the aim of continuing of the project. The Vajont is definitely a case of the latter.

The dam was built as a result of industrialisation and during the aftermath of the Second World War. The aim was to provide jobs and development to the region. These aspirations put pressure on the project of building the dam, as well as maximising the utilisation of it. This was the main driving factor to the construction of the dam. It was definitely a good idea to improve the welfare for the people living around the valley. However, the decision to build the dam could be considered highly unethical due to the enormity of the risks involved. To put people's lives on the line for jobs and development in the region despite the vast amount of warnings signs was unethical.

It was highly unclear whether it was SADE, the government or individuals who were responsible for the disaster. The confusion of who was held accountable enabled for decision making which was purely based on economic incentives, whereas voices from the communities and scientific expertise were neglected. Therefore, there was capacity for better decision-making, however, the potential was not exploited.

6. Conclusion

The purpose of this thesis has been to study the origins of failure and the filling-drawdown effects of the Vajont slide by performing a literature review. In addition, to create a broader understanding of the problem different analyses have been carried through such as; 1) mechanical sliding; 2) hydromechanical sliding; and 3) thermomechanical sliding.

In the case of Vajont the origins of the failure were closely linked to the existence of an ancient landslide. The slope of Mt. Toc was already unstable before the construction of the dam and the prehistoric landslide contributed to the enormous magnitude of the disaster. There are many aspects that played a part in the event of the landslide such as the effect of precipitation, thermal softening and the filling drawdown-effects. Since the contributing factors are many and they all intertwine with each other, it is very intricate to pinpoint the exact reason for the origins of failure. Hence research regarding multiphysical coupling between the effects is required and is a subject for further studies.

The case comparison generated different results since all of them were very different in terms of input parameters and had individual methods of calculation. However, they all shared the fundamental relationships between the mass, acceleration, driving and resisting forces. The most extensive results were from the case of hydromechanical sliding. The case of hydromechanical sliding was the most comprehensive method since it considered numerous parameters such as the effect of friction angle, rapid drawdown, hydrostatic water pressure, cohesion and uplift force. Based on the results the effect of water had a crucial impact on the stability of the slope of Vajont.

There were many indications proving that the landslide was unstable. However, these warning signs were neglected. The reasons for this were conflicting ideas of the actors involved such as differences in political interests. However, if the indications of the landslide had been more conclusive at the time the decision-making might have taken another route. At present-day there are several techniques to monitor landslides, which hopefully contributes to more reliable way of decision-making. Nonetheless in the case of Vajont the collection of data is still difficult from a practical point of view and very expensive despite the usage of modern standards.

In summary the catastrophe of the Vajont slide could likely not have been avoided. However, the consequences of the landslide could have been controlled in a better way. It is possible that the implementation of modern standards, further extensive geotechnical studies and the involvement of critical opinions proposed by researchers would have led to an early evacuation. As a result, preventive measures could have been taken into account at an earlier stage to save the lives of innocent people.

References

A. Al-Anboori & J-M. Kendall. (2010). Passive Seismic Monitoring of Reservoirs: A Case Study from Oman. In D. H. Johnston (Ed.), *Methods and Applications in Reservoir Geophysics*, (s.441-450). Tulsa: Society of Exploration Geophysicists.

Abbaszadeh, S., & Rastiveisa, H. (2017). A COMPARISON OF CLOSE-RANGE PHOTOGRAMMETRY USING A NON-PROFESSIONAL CAMERA WITH FIELD SURVEYING FOR VPLUME ESTIMATION. *International Archives of the Photogrammetry, Remote Sensing and Spatial Information Sciences*, *42*(4/W4). doi: doi.org/10.5194/isprs-archives-XLII-4-W4-1-2017

Alonso, E. E., Pinyol, N. M. & Puzrin, A. M. (2010). *Geomechanics of Failure, Advanced Topics*. Chapter 2 - Catastrophic Slide: The Vaiont Landslide, Italy. Springer Science and Business Media B.V.

Barrotta, P., & E, Montuschi. 2018. "The Dam Project: Who are experts? A Philosophical Lesson from the Vajont Disaster." In P. Barrotta and G. Scarafile (Ed.), *Science and Democracy. Controversies and Conflicts*, (p. 17-33). Amsterdam: Benjamins.

Bianchizza, C., & Frigerio, S. I. M. O. N. E. (2013). Domination of or adaptation to nature? A lesson we can still learn from the Vajont. *Ital. J. Eng. Geol. Environ*, *6*, 523-531.

Bolla, A, Paronuzzi, P. (2012). The Prehistoric Vajont Rockslide: An updated geological model. *Elsevier, 169-170*, 165-191. doi: 10.1016/j.geomorph.2012.04.021

Cai, Y.J. Cojean, R. (2011). Analysis and Modeling of slope stability in three-gorges dam reservoir (China) - The Case of Huangtupo landslide. *Science press and institute of Mountain Hazards and Environment, 8*, 166-175. doi: 10.1007/s11629-011-2100-0.

Chen, Y.M., Fredlund, D.G., Jia, G.W., Zhan, L.T. (2009). Performance of a large-scale slope model subjected to rising and lowering water levels. *Engineering Geology, 106*, 92-103. Gathered from: https://ac.els-cdn.com/S0013795209000544/1-s2.0-S0013795209000544-main.pdf?_tid=3ec44dc1-7710-4e3e-a7c3-6c63d6a38528&acdnat=1551964794_43ea1d90bb2915bda6381276d9d0e32a

Cheremisinoff, N. P. (1998). *Groundwater remediation and treatment technologies.* New Jersey: Noyes publications.

Chernov, D., & Sornette, D. (2016). Examples of risk information concealment practice. In *Man-made Catastrophes and Risk Information Concealment* pp. 9-245. Cham: Springer.

Choo, J. & Sun, W. (2018). Coupled phase-field and plasticity modeling of geological materials: From brittle fracture to ductile flow. *Computer Methods in Applied Mechanics and Engineering, 330*, 1-32. doi: 10.1016/j.cma.2017.10.009

Craig, R. F, & Knappet, J. A. (2012). *Craig's soil mechanics*. London & New York: Spon press.

Crosta, G. B., Imposimato, S., & Roddeman, D. (2016). Landslide spreading, impulse water waves and modelling of the Vajont rockslide. *Rock Mechanics and Rock Engineering*, *49*(6), 2413-2436.

Eberhardt, E., Stead, D., Karami, A., & Coggan, J. (2004, October). Numerical analysis of brittle fracture propagation and step-path failure in massive rock slopes. In *57th Canadian Geotechnical Conference, 5th Joint CGS/IAH-CNC Conference, Quebec City*.

G. Fripo, R. Salvini, M. Francioni, P.G. Ranjith. (2011). Use of Digital Terrestrial Photogrammetry in rocky slope stability analysis by Distinct Elements Numerical Methods. *International Journal of Rock Mechanics and Mining Sciences, 48*, 1045-1054. doi.org/10.1016/j.ijrmms.2011.07.007

Genevois, R. & Ghirotti, M. (2005). The 1963 Vaiont Landslide. *Giornale di Geologia Applicata, 1*, 41-52. doi: 10.1474/GGA.2005-01.0-05.0005

Genevois, R., & Tecca, P. R. (2013). The Vajont landslide: state-of-the-art. *Italian journal of Engineering Geology and Environment, 6*, 15-39. doi: 10.4408/IJEGE.2013-06. B-02

Gudmundsson, A. (2011). Theories of brittle failure of rocks. In *Rock Fractures in Geological Processes* pp. 190-232. Cambridge: Cambridge University Press. doi:10.1017/CBO9780511975684.008

Habib, P. (1975). Production of gaseous pore pressure during rock slides. *Rock mechanics, 7* (4), 193-197. doi: https://doi.org/10.1007/BF01246865

Havaej, M., Wolter, A., & Stead, D. (2015). The possible role of brittle rock fracture in the 1963 Vajont Slide, Italy. *International Journal of Rock Mechanics and Mining Sciences, 78*, 319-330.

Highland, L., & Bobrowsky, P. T. (2008). *The landslide handbook: a guide to understanding landslides*. Reston: US Geological Survey.

Huang, M. Jia, C. Q. (2009). Strength reduction FEM in stability analysis of soil slopes subjected to transient unsaturated seepage. *Computers and geotechnics, 36*, 93-101. doi: 10.1016/j.compgeo.2008.03.006

Huang, Y. H. (2013). *Slope stability analysis by the limit equilibrium method: fundamentals and methods*. American Society of Civil Engineers (ASCE).

Johansson, J.M.A. (2014) *Impact of Water-Level Variations on Slope Stability*. (Licentiate thesis) Luleå: Institutionen för samhällsbyggnad och naturresurser. Retrieved from: https://www.diva-portal.org/smash/get/diva2:999168/FULLTEXT01.pdf

Kilburn, C. R., & Petley, D. N. (2003). Forecasting giant, catastrophic slope collapse: lessons from Vajont, Northern Italy. *Geomorphology*, *54*(1-2), 21-32.

Kinematik. (2019). In *Nationalencyklopedin.* Retrieved 2019-05-12 from: https://www.ne.se/uppslagsverk/encyklopedi/l%C3%A5ng/kinematik

Li, J.C., Liu, Q.Q (2015). Effects of water seepage on the stability of soil-slopes. *Procedia IUTAM, 17*, 29-39. doi: 10.1016/j.piutam.2015.06.006

Mantovani, F. & Vita-Finzi, C. (2003). Neotectonics of the Vajont dam site. *Geomorphology*, *54*(1-2), 33-37. Doi: https://doi.org/10.1016/S0169-555X(03)00053-9.

Marco, D. R. (2012). Decision-making errors and socio-political disputes over the Vajont dam disaster. *Disaster advances*, *5*(3), 144-152.

Marzocchi, W., Murru, M., Lombardi, A. M., Falcone, G., & Console, R. SOME INSIGHTS ABOUT THE RELATION AMONG SEISMIC ACTIVITY, TECTONIC STRUCTURES AND ROCKSLIDE KINEMATICS AT THE VAJONT DAM SITE. *Bulletin of the Seismological Society of America*, *94*(1), 88-98.

Massironi, M., Zampieri, D., Superchi, L., Bistacchi, A., Ravagnan, R., Bergamo, A., Ghirotti, M., & Genevois, R. (2013). Geological structures of the Vajont landslide. *Thoughts and analyses after 50 years since the catastrophic landslide*, *1*, 573-882. doi: 10.4408/IJEGE.2013-06.B-55.

Müller-Salzburg, L. (1986). The Vajont slide. *Engineering Geology*, *24*, 513-523.

Pariseau, W. G. (2011). *Design Analysis in Rock Mechanics*. Boca Raton: Taylor & Francis Group

Paronuzzi, P., Bolla, A. & Rigo, E. (2016). Brittle and Ductile Behavior in Deep-Seated Landslides: Learning from the Vajont Experience. *Rock Mechanics and Rock Engineering*, *49*(6), 2389-2411. doi: https://doi.org/10.1007/s00603-015-0815-x

Paronuzzi, P., Rigo, E., & Bolla, A. (2013). Influence of filling–drawdown cycles of the Vajont reservoir on Mt. Toc slope stability. *Geomorphology*, *191*, 75-93.

Petley, D. (2008, 11 December). *The Vaiont (Vajont) landslide of 1963* [Blog post]. Retrieved from https://blogs.agu.org/landslideblog/2008/12/11/the-vaiont-vajont-landslide-of-1963/

Petley, D. N. (1999). Failure envelopes of mudrocks at high confining pressures. *Geological Society, London, Special Publications*, *158*(1), 61-71. doi: https://doi.org/10.1144/GSL.SP.1999.158.01.05

Petley, D. N., & Allison, R. J. (1997). The mechanics of deep-seated landslides. *Earth Surface Processes and Landforms: The Journal of the British Geomorphological Group*, *22*(8), 747-758.

Pinyol, N. M. & Alonso, E. E., (2010). Criteria for rapid sliding II: Thermo-hydro-mechanical and scale effect in Vaiont case. *Engineering Geology*, *114*, (3-4), 211-227. doi: https://doi.org/10.1016/j.enggeo.2010.04.017.

Prokešová, R., Medveďová, A., Tábořík, P., & Snopková, Z. (2013). Towards hydrological triggering mechanisms of large deep-seated landslides. *Landslides*, *10*(3), 239-254.

R. A. Beddoe & W. A. Take. (2015). Influence of slope inclination on the triggering and distal reach of hydraulically-induced flow slides. *Engineering Geology*, *187*, 170-182. doi.org/10.1016/j.enggeo.2015.01.006

Regenauer-Lieb, K., Hobbs, B., Ord, A., & Yuen, D. A. (2007). Non-equilibrium Thermodynamics, Thermomechanics, Geodynamics. In *International Conference on Computational Science*, 2017, Berlin, 62-69. doi: 10.1007/b137725

Rossi, N., & Toniolo, G. (1996). Italy. In N. Crafts & G. Toniolo (Eds.), *Economic Growth in Europe since 1945*. Cambridge: Cambridge University Press. doi:10.1017/CBO9780511758683.015

Säkerhetsfaktor. (2019). *Nationalencyklopedin*. Retrieved from: http://www.ne.se/uppslagsverk/encyklopedi/lång/säkerhetsfaktor

Sällfors, G. (2013). *Geoteknik*. Göteborg: Cremona Förlag.

Scaioni, M. (2015). *Modern Technologies for Landslide Monitoring and Prediction*. Berlin: Springer.

Semenza, E. & Ghirotti, M. (2000). History of the 1963 Vaiont slide: the importance of geological factors. *Bulletin of Engineering Geology and the Environment, 59*(2), 87-97. doi: https://doi.org/10.1007/s100640000067

Stead, D. & Eberhardt, E. (2013). Understanding the mechanics of large landslides. *Italian Journal of Engineering and Environment - Book Series, 6*, 85-112.

Voight, B., & Faust, C. (1982). Frictional heat and strength loss in some rapid landslides. *Geotechnique, 32*(1), 43-54.

Waldron, K. J., Kinzel, G. L., & Agrawal, S. K. (2016). *Kinematics, dynamics, and design of machinery*. Retrieved from http://search.ebscohost.com/login.aspx?direct=true&db=cat06296a&AN=clc.b2487362&site=eds-live&scope=site

Wolter, A., Stead, D., Ward, B. C., Clague, J. J., & Ghirotti, M. (2019). Engineering geomorphological characterisation of the Vajont Slide, Italy, and a new interpretation of the chronology and evolution of the landslide. *Landslide, 13*(5), 1067–1081. doi:10.1007/s10346-015-0668-0

Yang, H., Rahardjo, H. Xiao, D. (2010). Rapid Drawdown of Water Table in Layered Soil column. Qiang, H. Shui-Long, S. (Ed.) *In Geoenvironmental engineering and geotechnics: progress in modelling and applications.* (202-209). Shanghai, China: American society of Civil Engineers (ASCE).

Bibliography

Montagna, R. (2005). *The area of the 1963 landslide on Monte Toc, taken in 2005* [Electronic image]. Retrieved from: https://en.wikipedia.org/wiki/Vajont_Dam

VENET01. (2018). *Diga Vajont colori, taken in 2018* [Electronic image]. Retrieved from: https://upload.wikimedia.org/wikipedia/commons/8/8e/Diga_Vajont_colori_%28bromocolor%29.jpg